

Hidden Lagrangian coherence and memory effects in the statistics of Hamiltonian motions

Madalina Vlad, Dragos Iustin Palade, Florin Spineanu^{1,*}

¹*National Institute of Laser, Plasma and Radiation Physics, Magurele, Romania*

1. INTRODUCTION

Turbulence is a complex nonlinear process, which appears in many domains as fluid mechanics, plasma physics, astrophysics, atmosphere and ocean sciences, chemistry [1]-[3]. One of the main difficulty in understanding the dynamics of turbulence is the complicated combination of stochastic and quasi-coherent aspects that is typical for the strongly nonlinear regimes.

Quasi-coherence or order appears at the basic level of tracer trajectories in smooth stochastic velocity fields with finite correlation lengths λ and times τ_c . Trajectory coherence (or Lagrangian coherence) is usually a transitory process that lasts during the time of flight over λ with the amplitude V of the stochastic velocity, $\tau_{fl} = \lambda/V$. It exists only for slow time variation of the velocity with $\tau_c > \tau_{fl}$. In the case of two-dimensional incompressible velocity fields, a much stronger Lagrangian coherence appears that is due to trajectory eddying or trapping. It generates vortical structures of trajectories, which produce non-Gaussian statistics of tracer displacements and strongly modified transport [4]-[7]. The order of the tracer trajectories determines much more complicated effects on turbulence evolution, which essentially amplifies the degree of quasi-coherence. The turbulence that is dominantly two-dimensional has a self-organizing character [8]-[11], which consists of the generation of quasi-coherent large scale structures [12].

This paper is focused on the coherent effects that appear in tracer statistics in two-dimensional incompressible turbulence in the presence of an average velocity \mathbf{V}_d . We show that \mathbf{V}_d determines strong modifications of the transport and trajectory statistics, which are essentially caused by hidden coherent components of the motion.

The results are based on the numerical simulation of the trajectories and consist of a conditional statistical analysis adapted to the special properties of the two-dimensional incompressible velocity fields.

The formulation of the problem and the simulation method are presented in Section 2. The motion is of Hamiltonian type with the Hamiltonian function ϕ_t composed of the stochastic and average potentials. The trajectories evolve on the contour lines of $\phi_t(\mathbf{x})$ in static (frozen) potentials ($\tau_c \rightarrow \infty$), and they remain strongly correlated to these lines for slow time variation (large τ_c). We consider first (Sections 3-5) frozen potentials. We discuss the configuration of the contour lines of the potential and the main features of tracer advection in Section 3. The space of trajectories is organized in two categories: trapped and free. The statistics of the Lagrangian velocity and of the trajectories are examined for each category, and their specific contributions to the global statistics (on the whole set of trajectories) are identified (Section 4). We show that quasi-coherent Lagrangian velocities parallel to \mathbf{V}_d are generated for both categories. They are hidden in the global statistics, in the sense that their contributions compensate each other. However, they provide explanations for the nonstandard transport produced in these conditions. A deeper examination of the coherence induced by the average velocity is presented in Section 5, where we determine the Lagrangian statistics for the trajectories of each category that evolve on contour lines of the potential with the same value of ϕ_t . These results reveal other (hidden) coherent elements of the motion, and provide important properties that are used for the understanding of the effects of the average velocity on the statistics of trajectories and transport. Sections 6 and 7 deal with time dependent potentials. The Lagrangian statistics conditioned by the value of the potential shows that the order found in frozen potentials does not decay due to the random time variation of the potential, as expected. On the contrary, important quasi-coherent elements significantly increase (Section 6). Explanations are provided in Section 7. They are essentially related to the constraint of invariance of the potential, which are approximately valid at large τ_c , and to the slow transition of the trajectories between the two categories. Long memory effects are identified and their effects is discussed. A short summary of the results and the conclusions are presented in Section 8.

2. THE PROBLEM AND THE SIMULATION METHOD

Tracer trajectories in two-dimensional stochastic velocity fields are obtained from

$$\frac{d\mathbf{x}}{dt} = \mathbf{v}(\mathbf{x}, t) = \tilde{\mathbf{v}}(\mathbf{x}, t) + V_d \mathbf{e}_2, \quad (1)$$

where $\mathbf{e}_1, \mathbf{e}_2$ are the unit vectors in the plane of the motion $\mathbf{x} = (x_1, x_2)$, \mathbf{e}_3 is perpendicular on this plane. The velocity $\mathbf{v}(\mathbf{x}, t)$ has a stochastic component $\tilde{\mathbf{v}}(\mathbf{x}, t)$ superposed on a constant average velocity $\mathbf{V}_d = V_d \mathbf{e}_2$. The incompressibility condition $\nabla \cdot \tilde{\mathbf{v}}(\mathbf{x}, t) = 0$ of the velocity field is equivalent with the representation of $\tilde{\mathbf{v}}(\mathbf{x}, t)$ by a stochastic potential (or stream function) $\phi(\mathbf{x}, t)$

$$\tilde{\mathbf{v}}(\mathbf{x}, t) = -\nabla \phi(\mathbf{x}, t) \times \mathbf{e}_3. \quad (2)$$

The equation of motion is of Hamiltonian type, with x_1 and x_2 the conjugate variables and $\phi_t(\mathbf{x}, t) = \phi(\mathbf{x}, t) + x_1 V_d$ the Hamiltonian function.

Dimensionless quantities are used in Eq. (1) with the potential normalized by its amplitude Φ , the distances by λ_0 that is of the order of the correlation lengths, the velocities (including V_d) by $V_0 = \Phi/\lambda_0$ and the time by $\tau_0 = \lambda_0/V_0$.

The potential is represented by a homogeneous and stationary Gaussian stochastic field. Its Eulerian correlation (EC) $E(\mathbf{x}, t) \equiv \langle \phi(\mathbf{x}_0, t_0) \phi(\mathbf{x}_0 + \mathbf{x}, t_0 + t) \rangle$ in dimensionless quantities is modeled in the simulations presented here by

$$E(\mathbf{x}, t) \equiv \exp\left(-\frac{x_1^2}{2\lambda_1^2} - \frac{x_2^2}{2\lambda_2^2} - \frac{t^2}{2\tau_c^2}\right), \quad (3)$$

where λ_i are the correlation lengths of the 2-dimensional potential and τ_c is the correlation time. The EC's of the velocity components $E_{ii}(\mathbf{x}, t) \equiv \langle v_i(\mathbf{x}_0, t_0) v_i(\mathbf{x}_0 + \mathbf{x}, t_0 + t) \rangle$ are

$$E_{11}(\mathbf{x}, t) = -\partial_2 \partial_2 E(\mathbf{x}, t), \quad E_{22}(\mathbf{x}, t) = -\partial_1 \partial_1 E(\mathbf{x}, t), \quad (4)$$

which determine the normalized amplitudes of the velocity fluctuations $V_1 = \sqrt{E_{11}(\mathbf{0}, 0)} = 1/\lambda_2$, $V_2 = 1/\lambda_1$.

The statistical properties of the trajectories obtained from Eq. (1) are numerically analyzed. More precisely, we determine the statistics of the trajectories and of the Lagrangian velocity, and a class of conditional Lagrangian correlations that reveal the quasi-coherent components of the motion and their properties.

We use statistical averages, which consists of generating a large number of realizations (r) of the stochastic Gaussian potential and of determining the trajectory with the initial condition $\mathbf{x}(0) = \mathbf{0}$ in each r by effectively computing the velocity on the trajectory at each time step, $\mathbf{v}(\mathbf{x}(t_i), t_i)$. However, the analysis of the results is connected to the equivalent space averaging procedure. This corresponds to the statistical ensemble of trajectories obtained in a single typical realization of the potential by different initial conditions $\mathbf{x}(0) = \mathbf{x}_0^r$, where the points \mathbf{x}_0^r are uniformly distributed in a very large domain.

We use the simulation code presented in [13], which is based on a fast generator of Gaussian fields with prescribed spectra. In the present work, we have implemented the so called FRD representation

$$\phi(\mathbf{X}) = \sum_{i=1}^{N_c} \sqrt{S(\mathbf{K}_i)} \sin\left(\mathbf{K}_i \mathbf{X} + \frac{\pi}{4} \zeta_i\right), \quad (5)$$

where $\mathbf{X} \equiv (\mathbf{x}, t)$ is the three-dimensional space-time and $\mathbf{K}_i \equiv (\mathbf{k}_\perp^i, \omega^i)$ are the N_c discrete values of the wave numbers \mathbf{k}_\perp^i and frequencies ω^i . $S(\mathbf{K})$ is the spectrum of the stochastic potential, the Fourier transform of the EC (3). This representation is different of the usual discrete Fourier decomposition by the set of the values of \mathbf{K}_i that are not the fixed points of a three-dimensional mesh, but random values with uniform distribution. Also, the random phases ζ_i have not continuous distributions, but discrete values ± 1 (with equal probabilities).

Each set of the N_c random values of \mathbf{K}_i and ζ_i determines a realization r of the potential and a trajectory (solution of Eq. (1) with initial condition $\mathbf{x}(0) = \mathbf{0}$). The statistical ensemble R consists of a number M of these sets.

The representation (5) provides a fast convergence of the Eulerian properties of the stochastic potential. We have shown that reasonable errors in the EC and in the probability of the potential are obtained at much smaller values of N_c and M than in the usual fast Fourier representation (FFR). This leads to the decrease of the computing times by roughly one order of magnitude compared to the usual FFR method in two-dimensional potentials [13]. Most of the simulations analyzed here are performed with $N_c = 500$ and $M = 10^5$.

3. MAIN FEATURES OF TRACER ADVECTION

The incompressibility of the two-dimensional velocity field ($\nabla \cdot \mathbf{v}(\mathbf{x}, t) = 0$) determines two invariance laws of the solutions of Eq. (1). It leads to equations of motion of Hamiltonian type, with x_1 and x_2 conjugate variables and ϕ_t the Hamiltonian function. In the case of time independent (frozen) potentials $\phi(\mathbf{x})$, the trajectories are linked to the contour line of the potential $\phi_t(\mathbf{x})$, which means that the Lagrangian potential $\phi_t(\mathbf{x}(t))$ is invariant along each trajectory. The other invariant law is statistical and applies to the motion in both frozen and time dependent potentials $\phi_t(\mathbf{x}(t), t)$ for any value of the correlation time τ_c . It concerns the distribution of the Lagrangian velocity $\mathbf{v}(\mathbf{x}(t), t)$, that is shown to be time independent, and thus identical with the distribution of the Eulerian velocity $\mathbf{v}(\mathbf{x}, t)$. The Lagrangian potential is statistically invariant too. This property is trivial in frozen potentials where $\phi_t(\mathbf{x}(t)) = \phi_t(\mathbf{x}(0))$ and it is similar to the case of the velocity in time dependent potentials where $\phi_t(\mathbf{x}(t), t)$ changes in time.

An example of configuration of the contour lines of the potential can be seen in Fig. 1, where a typical realization of $\phi_t(\mathbf{x})$ is presented for $V_d = 0$ (left panel) and for $V_d = 0.3$ (right panel). The contour lines at $V_d = 0$ are nested closed curves with multi-scale sizes that have the dimensions r_{\max} from $r_{\max} \ll \lambda_i$ to $r_{\max} \rightarrow \infty$. The average velocity \mathbf{V}_d completely changes the field lines by breaking the large size contour lines and generating (winding) open paths along its direction. Islands of closed contour lines remain between the network of open paths, but their average size decreases as V_d increases, and, for V_d much larger than the amplitude of the stochastic velocity, all the lines are open. The average velocity also determines the limitation of the excursion of the contour lines perpendicular to \mathbf{V}_d .

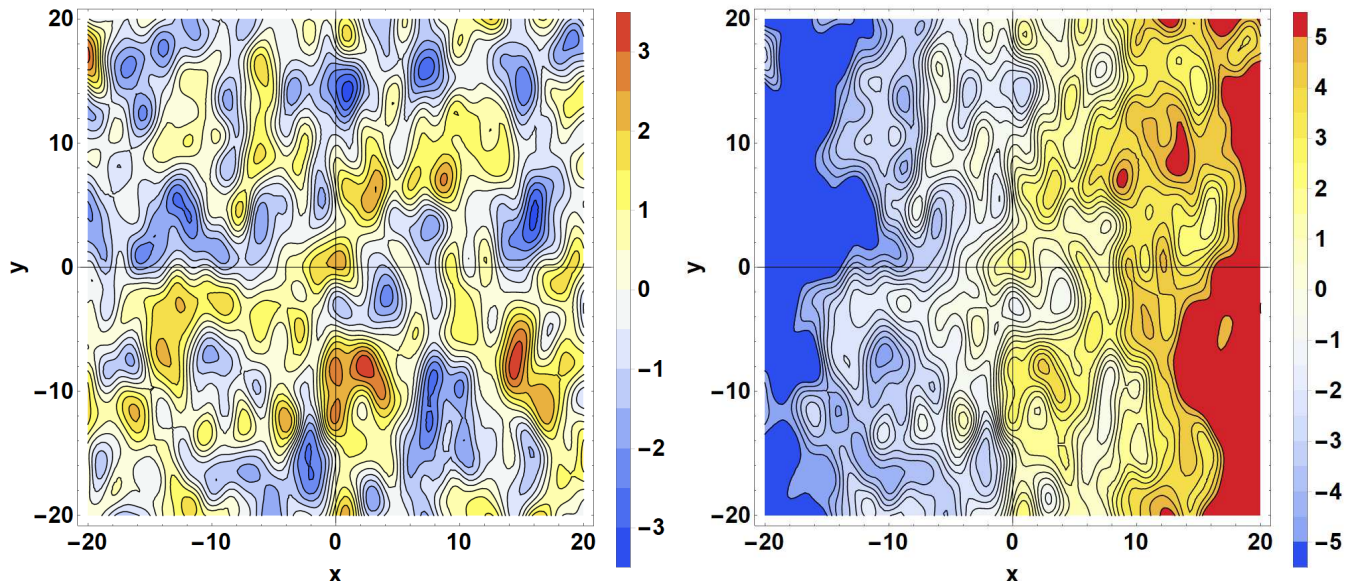


FIG. 1: Typical realization of the potential $\phi_t(\mathbf{x})$ for $V_d = 0$ (left panel) and for $V_d = 0.3$ (right panel).

This configuration of the contour lines of $\phi_t(\mathbf{x})$ determines solutions of Eq. (1) that are, in the presence of an average velocity, a mixture of localized periodic (or trapped) trajectories that are closed, and of free trajectories that have unlimited displacements along \mathbf{V}_d . The space of trajectories R is organized in two disjointed subensembles: tr for the trapped trajectories and fr for the free ones ($R = tr \cup fr$, $tr \cap fr = \emptyset$). The classification criterion is the periodicity of the trajectories. A trajectory r with period T_r belongs to tr if T_r is finite and to fr otherwise. T_r is defined as the time of the first return in the initial point $\mathbf{x}(0) = \mathbf{0}$, and is determined as the first solution of $r(t) = 0$, where $r(t) = \sqrt{x_1^2(t) + x_2^2(t)}$. Practically, a trajectory belongs to the subensemble tr when its period is smaller than the time of integration t_{\max} . The size of each trajectory $r_{\max} = \text{Max}(r(t))$ is also calculated.

For $V_d = 0$, all trajectories $\mathbf{x}(t)$ are closed, periodic functions of time when $t \rightarrow \infty$. At finite time t , open trajectories are found, which correspond to large periods $T_r > t$ (and to large size contour lines). As t increases the fraction of free trajectories decreases, and, in the limit $t \rightarrow \infty$, all trajectories are trapped ($tr = R$ and $fr = \emptyset$). The probability of trajectory sizes $P(r_{\max}, t)$ is represented in Fig. 2 at two time moments, $t = 60$ (dashed line) and $t = 120$ (solid line). One can see that the time evolution of $P(r_{\max}, t)$ affects only the large distances, while the small r_{\max} domain has invariant probability. The contributions of the closed and open trajectories to $P(r_{\max}, t)$ are also represented

in the figure. The closed trajectories (red points) determine the invariant part of $P(r_{\max}, t)$. The open trajectories (green points) have large sizes and they determine the time variation of $P(r_{\max}, t)$. Their contribution move toward larger r_{\max} as time increases and it decays, such that $P(r_{\max}, t)$ is determined only by closed trajectories in the limit $t \rightarrow \infty$. It is a decaying function of r_{\max} that scales as $P(r_{\max}, t) \sim r_{\max}^{-1.3}$ at large t . The slow algebraic decay of the asymptotic probability shows that the sizes of the trajectories cover multiple scales from $r_{\max} \ll \lambda_i$ to $r_{\max} \rightarrow \infty$.

Thus, the invariance of the Lagrangian potential determines a process of trajectory trapping manifested by eddying in the structure of $\phi(\mathbf{x})$.

The average velocity V_d that strongly modifies the structure of the field lines of $\phi_t(\mathbf{x})$ determines a significant change of the probability of trajectory sizes. Two categories of trajectories coexist for $V_d \lesssim V$: periodic, closed trajectories situated on the islands of closed contour lines of $\phi_t(\mathbf{x})$ and non-periodic trajectories along the open paths generated by the average potential xV_d . The latter are free trajectories that make large displacements along \mathbf{V}_d . The probability $P(r_{\max}, t)$ can be written as the sum of the contributions of these two types of trajectories

$$P(r_{\max}, t) = n_{tr}(r_{\max}, t) + n_{fr}(r_{\max}, t), \quad (6)$$

where n_{tr} , n_{fr} are determined in the subensembles tr and fr at time t . $P(r_{\max}, t)$, shown in Fig. 3 (left panel) has a second maximum. It appears at a large value of r_{\max} that increases with the increase of V_d . Also, the amplitude and the width of this peak increase with V_d . It is determined by the free trajectories. The narrow peak $n_{tr}(r_{\max}, t)$ at small r_{\max} is the contribution of the trapped, periodic trajectories. It is represented in the right panel of Fig. 3, which shows that both the maximum size and the amplitude of the trapped trajectories decrease as V_d increases. The average velocity hinders and eventually eliminates the trapping process. The contribution $n_{tr}(r_{\max}, t)$ in Eq. (6) decreases with V_d and become negligible at $V_d \gg 1$. The contribution of the free trajectories is negligible in this range of small sizes, at any V_d , as shown in Fig. 3 (right panel) where the black points for $P(r_{\max}, t)$ are superposed on the red curves for $n_{tr}(r_{\max}, t)$. The two contributions in Eq. (6) separates at large time.

The probability of the periods of the closed trajectories $P(T, t)$ calculated from the trajectories $\mathbf{x}(t)$ at $t = 60$ is shown in Fig. 4. One can see that, at small V_d , this probability extends to large values of $T \lesssim 100$ and it has a weak decay. As V_d increases, the width of $P(T, t)$ decreases and its decay is steeper. This behavior is in agreement with the decay of the trajectory sizes at large V_d . An average velocity can be defined for the trapped trajectories as the maximum displacement over the period, $v^{eff} = r_{\max}/T$. Its probability is weakly dependent on the average velocity.

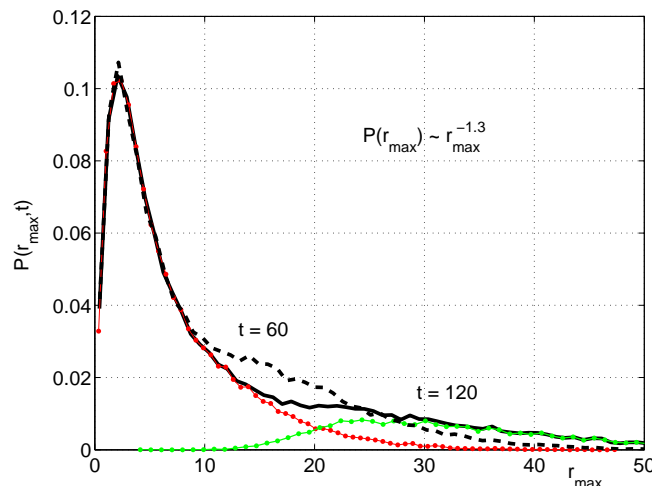


FIG. 2: The probability of trajectory sizes $P(r_{\max}, t)$ for $V_d = 0$ at $t = 60$ (dashed black line) and $t = 120$ (solid black line). Also shown are the contributions of the trapped (red points) and free (green points) trajectories at $t = 120$.

The fraction of trajectories that are not closed at time t , $n_{fr}(t, V_d)$ is obtained from the probability of the periods of the closed trajectories (calculated at the time of integration, t_{\max})

$$n_{fr}(t, V_d) = 1 - n_{tr}(t, V_d), \quad n_{tr}(t, V_d) = \int_0^t P(T, t_{\max}) dT. \quad (7)$$

This function decreases in time from $n_{fr}(0, V_d) = 1$, as seen in Fig. 5 (left panel). In the case $V_d \neq 0$, $n_{fr}(t, V_d)$ saturates at a value $n_{fr}(V_d)$ in a time that becomes shorter at larger V_d . In the case of $V_d = 0$, the decay is not limited, and it scales as $n_{fr}(t, 0) \sim t^{-0.6}$.

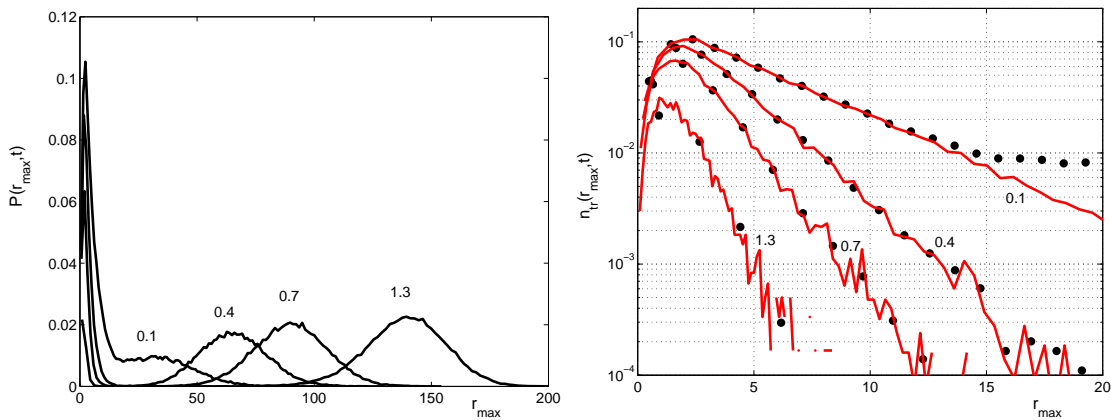


FIG. 3: The probability $P(r_{max}, t)$ for several average velocities V_d that label the curves, at $t = 60$ as function of r_{max} (the curves in the left panel and black points in the right panel) and the contribution of the trapped trajectories $n_{tr}(r_{max}, t)$ (right panel, red lines).

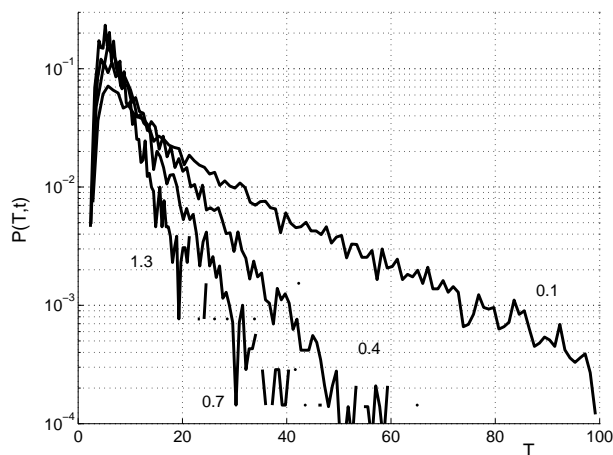


FIG. 4: The probability of the periods of the trapped trajectories $P(T, t)$ as functions of T at $t = 60$ and at the values of V_d that label the curves.

The results obtained for the asymptotic fraction of free trajectories $n_{fr}(V_d) \equiv \lim_{t \rightarrow \infty} n_{fr}(t, V_d)$, presented in Fig. 5 (right panel), are well approximated by

$$n_{fr}(V_d) = [1 - \exp(-V_d^2)]^{1/4}. \quad (8)$$

The fraction of trapped trajectories is $n_{tr}(t, V_d) = 1 - n_{fr}(t, V_d)$ at any time, with the asymptotic value $n_{tr}(V_d) = 1 - n_{fr}(V_d)$ that is also represented in Fig. 5 (right panel).

4. LAGRANGIAN STATISTICS IN STATIC POTENTIALS

Thus, the trajectories obtained in the stochastic potential $\phi_t(\mathbf{x})$ were divided into two categories: trapped and free. They have different topologies and different sizes, which suggests that their contributions to the global statistical properties of the trajectories are qualitatively different.

We analyze here the statistics of the Lagrangian velocity and of the displacements of each category of trajectories. For any Lagrangian quantity $A(\mathbf{x}(t))$, we determine $\langle A(\mathbf{x}(t)) \rangle_{tr}$ and $\langle A(\mathbf{x}(t)) \rangle_{fr}$ that are conditional averages restricted to the trapped and free trajectories, respectively. These are statistical averages calculated over the subspaces tr and fr . The contribution of each subensemble to the global average (over R) is the product of the probability that a trajectory belongs to the subensemble multiplied by the statistical average over the subensemble, $n_c(t, V_d) \langle A(\mathbf{x}(t)) \rangle_c$, where $c = tr, fr$. It yields

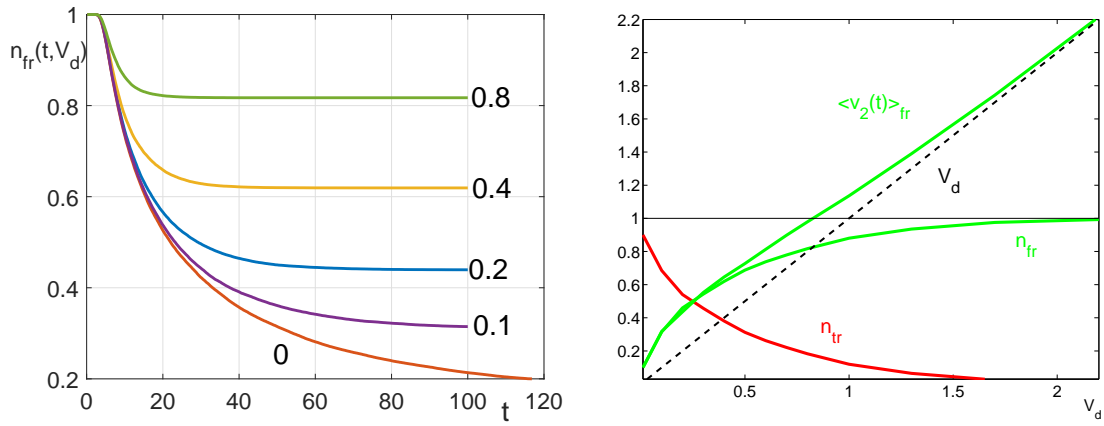


FIG. 5: Left panel: the fractions of free trajectories as function of time for the values of V_d that label the curves. Right panel: the asymptotic values n_{fr} and n_{tr} and the average velocity of the free trajectories (see next Section) as functions of V_d .

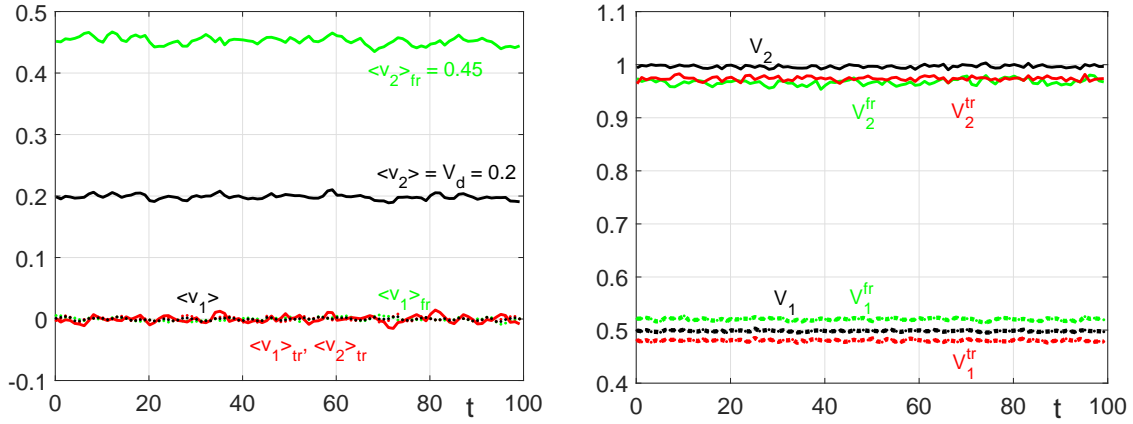


FIG. 6: The average Lagrangian velocities (left panel) and the fluctuations of the Lagrangian velocities (right panel) as functions of time. The dashed lines are for the v_1 and the solid lines for the v_2 . The green lines are for the free trajectories and the red lines for the trapped trajectories, while the black are averages on the whole statistical ensemble R . $V_d = 0.2$.

$$\langle A(\mathbf{x}(t)) \rangle = n_{tr}(t, V_d) \langle A(\mathbf{x}(t)) \rangle_{tr} + n_{fr}(t, V_d) \langle A(\mathbf{x}(t)) \rangle_{fr}. \quad (9)$$

The separation of the trajectories in these categories is performed at a large time such that $n_{fr}(t, V_d)$ is saturated (see Fig. 5, left panel).

4.1 Statistics of the Lagrangian velocity

The statistical parameters of the Lagrangian velocity $\mathbf{v}(\mathbf{x}(t)) \equiv \mathbf{v}(t)$ are shown in Fig. 6 for a stochastic potential with $\lambda_1 = 1$, $\lambda_2 = 2$ and $V_d = 0.2$. The average Eulerian velocity and fluctuation amplitudes are in this case $\langle v_1 \rangle = 0$, $\langle v_2 \rangle = V_d$, $V_1 = 0.5$ and $V_2 = 1$, where $V_i = \sqrt{\langle v_i^2 \rangle}$ are obtained from Eq. (4).

The Lagrangian quantities maintain the Eulerian values at any time, as stated by Lumley theorem. Besides this, the conditional average velocity and fluctuation amplitudes are time invariant, as seen in Fig. 6, but their values depend on the category.

It is interesting to note that the average velocity is determined only by the free trajectories, while the trapped trajectories do not contribute ($\langle v_2(t) \rangle_{tr} = 0$ at any time). The average velocity of the free trajectories is larger than V_d , and it can be approximated with

$$\langle v_2(t) \rangle_{fr} = \frac{V_d}{n_{fr}} > V_d \quad (10)$$

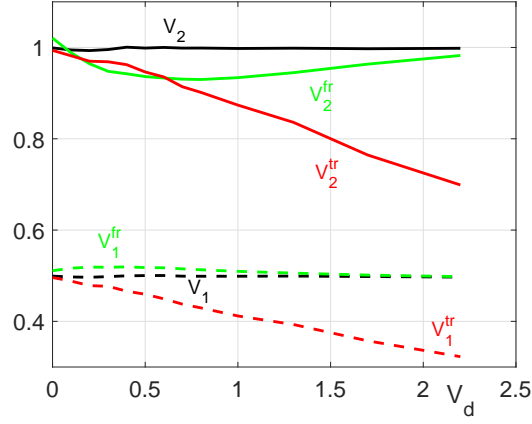


FIG. 7: The amplitudes of fluctuations of the Lagrangian velocities as functions of V_d . The dashed lines are for the v_1 and the solid lines for the v_2 . The green lines are for the free trajectories and the red lines for the trapped trajectories, while the black are averages on the whole statistical ensemble R .

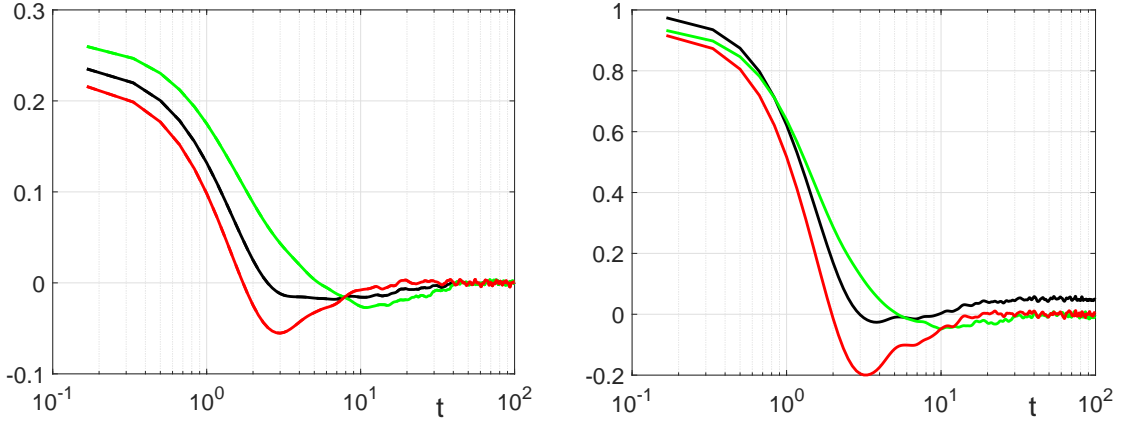


FIG. 8: The correlations of the Lagrangian velocity $v_1(t)$ (left panel) and $v_2(t)$ (right panel). The correlations on the whole statistical ensemble $L_i(t)$ (black lines) are compared to the subensemble correlations $L_i^{tr}(t)$ (red lines) and $L_i^{fr}(t)$ (green lines). $V_d = 0.2$.

It is $\langle v_2(t) \rangle_{fr} = 0.45$ for the example presented in Fig. 6, left panel, obtained for $V_d = 0.2$. The conditional average velocity $\langle v_2(t) \rangle_{fr}$ is also shown in Fig. 5 (right panel) as function of V_d . One can see that this average velocity is significantly larger than V_d only in the presence of trajectory trapping (for $V_d \lesssim 1$).

This result shows that a supplementary ordered component of the Lagrangian velocity appears for the free trajectories that exactly compensates the missing contribution of the trapped particles, such that $\langle v_2(t) \rangle = n_{fr} \langle v_2(t) \rangle_{fr} = V_d$. It seems to be a trivial consequence of $\langle v_2(t) \rangle_{tr} = 0$, but the underlying physical process is rather complex. It essentially consists of generation of ordered motion from the stochastic velocity $\tilde{\mathbf{v}}(\mathbf{x}, t)$ for both types of trajectories

$$\langle \tilde{v}_2(t) \rangle_{tr} = -V_d, \quad \langle \tilde{v}_2(t) \rangle_{fr} = V_d \frac{n_{tr}}{n_{fr}}. \quad (11)$$

The supplementary average velocity of the trapped trajectories is opposite to \mathbf{V}_d and exactly compensates it. The supplementary average velocity of the free trajectories is along \mathbf{V}_d and it contributes to the increase of the Lagrangian over the Eulerian velocity.

Equations (11) are valid at any time, including $t = 0$. It can be interpreted as the condition for the separation of the trajectories in the free and trapped categories. The trapped trajectories start from the geometric locus for which $\langle \tilde{v}_2(\mathbf{x}) \rangle = -V_d$ and they remain in this domain, while the free trajectories are confined in the complement of this domain. These ordered components of the motion are hidden, in the sense that they are not "seen" in the average velocity calculated on the whole ensemble R ($\langle v_2(t) \rangle = V_d$). However, as shown below, they have strong effects on the transport along \mathbf{V}_d through the modification of the correlation of the Lagrangian velocity.

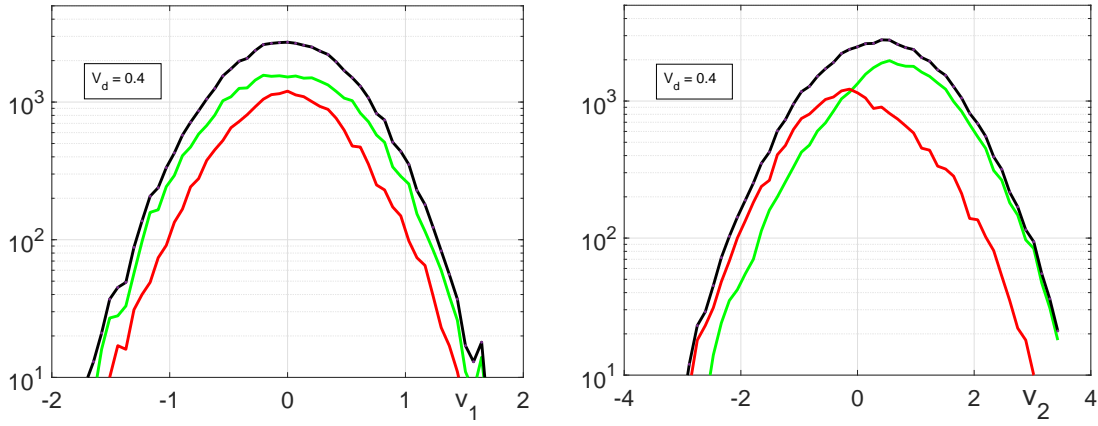


FIG. 9: Histograms of the Lagrangian velocities v_1 (left panel) and v_2 (right panel) represented by the black curves and the contributions determined by the free (green curves) and trapped (red curves) trajectories. $V_d = 0.4$.

The amplitudes of velocity fluctuations around the average velocity are shown in Fig. 6 (right panel). They are different for the two types of trajectories. It is interesting to underline that the supplementary order that characterizes trapped and free trajectories appears in the fluctuations of the velocity in R . The average of the square velocity decomposed on tr and fr subensembles according to Eq. (9) for large time

$$\langle v_i^2(t) \rangle = n_{tr} \langle v_i^2(t) \rangle_{tr} + n_{fr} \langle v_i^2(t) \rangle_{fr}, \quad (12)$$

leads to

$$V_2^2 = n_{tr}(V_2^{tr})^2 + n_{fr}(V_2^{fr})^2 + \frac{n_{tr}}{n_{fr}} V_d^2, \quad (13)$$

where

$$(V_i^c)^2 \equiv \langle (v_i(t) - \langle v_i(t) \rangle_c)^2 \rangle_c \quad (14)$$

are the amplitudes of the fluctuations of the velocity $\delta v_i(t) \equiv v_i(t) - \langle v_i(t) \rangle_c$, $i = 1, 2$, conditioned by the category of trajectories $c = tr, fr$ (on the subensembles tr and fr). Thus, a contribution produced by the ordered motion appears (the last term of Eq. (13)) besides the direct contributions of the conditional fluctuations. It is determined by the ordered motion (11) generated by V_d in the presence of trapping (for $V_d \lesssim 1$). The results presented in Fig. 6 (right panel) show values $V_2^{tr} < V_2$ and $V_2^{fr} < V_2$, which reproduce Eq. (13).

The conditioned amplitudes of the velocity fluctuations V_i^c depend on the average velocity V_d . As seen in Fig. 7, the amplitudes of both components of the trapped trajectory velocity (red curves) are continuously decreasing functions of V_d . This is the effect of the decrease of the size of the islands of closed contour lines of the potential, which, as V_d increases, shrink around the maxima and minima of $\phi(\mathbf{x})$ where the gradients are small. In the case of free trajectories (green lines), the amplitudes of the Lagrangian velocities are different of V_i only in the range of V_d that corresponds to the existence of islands of closed contour lines of the potential. The perpendicular amplitude is increased ($V_1^{fr} > V_1$), while the parallel amplitude is decreased ($V_2^{fr} < V_2$) such that the supplementary parallel velocity is compensated (Eq. (13)).

One can deduce from these results that the EC defined on the geometric locus of the free trajectories is different of the EC (3). As shown below (Section 6), the amplitude of the stochastic potential of the free trajectories Δ is smaller than in the whole space ($\Delta < \Phi$). The correlation lengths are evaluated using the amplitudes of velocity fluctuations of the free trajectories

$$\lambda_1^{fr} \sim \frac{\Delta}{V_2^{fr}} = \lambda_1 \frac{\Delta}{\Phi} \frac{V_2}{V_2^{fr}}, \quad \lambda_2^{fr} \sim \frac{\Delta}{V_1^{fr}} = \lambda_2 \frac{\Delta}{\Phi} \frac{V_1}{V_1^{fr}}, \quad (15)$$

where $\lambda_1 = \Phi/V_2$ and $\lambda_2 = \Phi/V_1$. Thus, the correlation lengths on the domain of free trajectories decrease with the factor Δ/Φ on both directions and are modified by the velocity amplitudes (decreased along \mathbf{V}_d and increased across \mathbf{V}_d).

The correlations of the Lagrangian velocity are shown in Fig. 8, where the notations are

$$L_i(t) = \langle \delta v_i(0) \delta v_i(t) \rangle, \quad L_i^c(t) = \langle \delta v_i(0) \delta v_i(t) \rangle_c, \quad c = tr, fr. \quad (16)$$

One can see that all the conditional correlations (for both categories and both components of the velocity) decay to zero at large t . However, the correlation of the velocity along \mathbf{V}_d calculated on all trajectories, $L_2(t)$, has a finite asymptotic value. It is determined by the ordered components of motion produced in subensembles tr and fr . An equation similar to (13) can be obtained from (9) written for $A = v_i(0) v_i(t)$

$$L_2(t) = n_{tr} L_2^{tr}(t) + n_{fr} L_2^{fr}(t) + \frac{n_{tr}}{n_{fr}} V_d^2, \quad (17)$$

which shows that $L_2(t)$ has a finite asymptotic tail in spite of the decay to zero of $L_2^{tr}(t)$ and $L_2^{fr}(t)$. It is determined by the presence of trapped trajectories at small average velocity V_d .

The histograms for the Lagrangian velocity components are time invariant for all statistical ensembles R , tr and fr . The histogram for all trajectories (in R) is shown in Fig. 9 together with the contributions of the trapped and free trajectories (that include the fractions of trajectories). One can see that the distribution is Gaussian in R , while significant departures from Gaussianity appear in the subensembles tr and fr , especially for the velocity component v_2 (right panel). The domain of large positive velocities is dominated by the free trajectories, while the trapped trajectories have the main contribution for the large negative v_2 . The most probable value of v_2 on tr (that is slightly negative) is compensated by a longer tail at positive v_2 .

The non-Gaussian distribution of the Lagrangian velocity of the trapped trajectories provides additional information on the geometric locus of this category of trajectories. It shows that the space average of the parallel velocity $v_2(\mathbf{x})$ on this locus (that is zero for any V_d) results from the elimination of the regions with large, positive $v_2(\mathbf{x})$. In other words, the regions where the stochastic velocity is oriented parallel to \mathbf{V}_d belong to the geometric locus fr .

4.2 Transport and statistics of trajectories

The statistics of the displacements is strongly non-Gaussian, in spite of the Gaussian Lagrangian velocity. Moreover, the average and mean square displacements (calculated for all trajectories and in the subensembles tr and fr) have asymptotic regimes that can be linear, quadratic or saturated functions of time, which shows that the transport has anomalous aspects.

The average displacements are in agreement with the average Lagrangian velocities

$$\begin{aligned} \langle x_1(t) \rangle &= \langle x_1(t) \rangle_{tr} = \langle x_1(t) \rangle_{fr} = 0, \\ \langle x_2(t) \rangle &= V_d t, \quad \langle x_2(t) \rangle_{tr} = 0, \quad \langle x_2(t) \rangle_{fr} = \frac{V_d}{n_{fr}} t. \end{aligned} \quad (18)$$

The dispersion $\langle (\delta x_i(t))^2 \rangle$, where $\delta x_i(t) = x_i(t) - \langle x_i(t) \rangle$ are shown in Fig. 10 for $V_d = 0$ (left panel) and for $V_d = 0.2$ (right panel), as functions of time.

In the absence of the average velocity ($V_d = 0$), the dispersions are similar along the two directions. The curves in the left panel of Fig. 10 are only translated due to the different amplitudes of the stochastic velocities $V_1 = 0.5$, $V_2 = 1$. The dispersions are sub-diffusive, with time increase that is slower than linear $\langle (\delta x_i(t))^2 \rangle \sim t^{0.68}$. The reason is the progressive saturation of the contributions of the trajectories with small periods. At a time t , all the trajectories with $T < t$ have saturated dispersion and only the free trajectories (that are still not closed) determine the time variation of $\langle (\delta x_i(t))^2 \rangle$. The latter results from two factors with opposite effects: the fraction of free trajectories at time t and their average size. As seen in Fig. 5, left panel, $n_{fr}(t, 0)$ is a decreasing function of time, $n_{fr}(t, 0) \sim t^{-0.6}$. The average size of the closed trajectories is an increasing function of t , because it is an increasing function of the average period.

The average velocity V_d makes trajectory dispersion strongly non-isotropic, as seen in Fig. 10, right panel. The dispersion $\langle (\delta x_i(t))^2 \rangle$ for all trajectories (black lines) are compared to the results obtained for the trapped $\langle (\delta x_i(t))^2 \rangle_{tr}$ (red lines) and free $\langle (\delta x_i(t))^2 \rangle_{fr}$ (green lines) trajectories. The dispersions across \mathbf{V}_d (of $x_1(t)$) for the whole set of trajectories and for the subensembles tr and fr are all saturated (the dashed curves in Fig. 10, right panel), which

corresponds to the minimum sub-diffusive transport. This means that the average velocity completely hinders the perpendicular transport in the case of static stochastic potentials. The contrary happens to the transport parallel to \mathbf{V}_d : the dispersion of the trajectories has a very fast time-increase, $\langle (\delta x_2(t))^2 \rangle \sim t^2$, which correspond to the maximum super-diffusive transport that is of the ballistic type. It appears in spite of the much weaker transport of the trapped and free trajectories ($\langle (\delta x_2(t))^2 \rangle_{tr}$ saturates and $\langle (\delta x_2(t))^2 \rangle_{fr} \sim t$ is diffusive).

This super-diffusive parallel transport is the effect of the coherent parallel motion generated by V_d , as demonstrated using Eq. (9) for $A = x_i^2(t)$. The relations between the dispersion of all trajectories (in R) and the subensemble tr and fr dispersions are

$$\langle (\delta x_1(t))^2 \rangle = n_{tr} \langle (\delta x_1(t))^2 \rangle_{tr} + n_{fr} \langle (\delta x_1(t))^2 \rangle_{fr}, \quad (19)$$

$$\langle (\delta x_2(t))^2 \rangle = n_{tr} \langle (\delta x_2(t))^2 \rangle_{tr} + n_{fr} \langle (\delta x_2(t))^2 \rangle_{fr} + \frac{n_{tr}}{n_{fr}} V_d^2 t^2. \quad (20)$$

The last term in Eq. (20) is dominant at large time and it makes the asymptotic regime superdiffusive of ballistic type. This term is determined by the supplementary average velocity generated from the stochastic components for the free and trapped trajectories, Eq. (11). It leads to the "concentration" of the average velocity along the free trajectories Eq. (10). Thus, the super-diffusive parallel transport is determined by the average velocity ($V_d \neq 0$) only in the presence of the islands of trapped trajectories ($n_{tr} \neq 0$), which corresponds to $V_d \lesssim 1$.

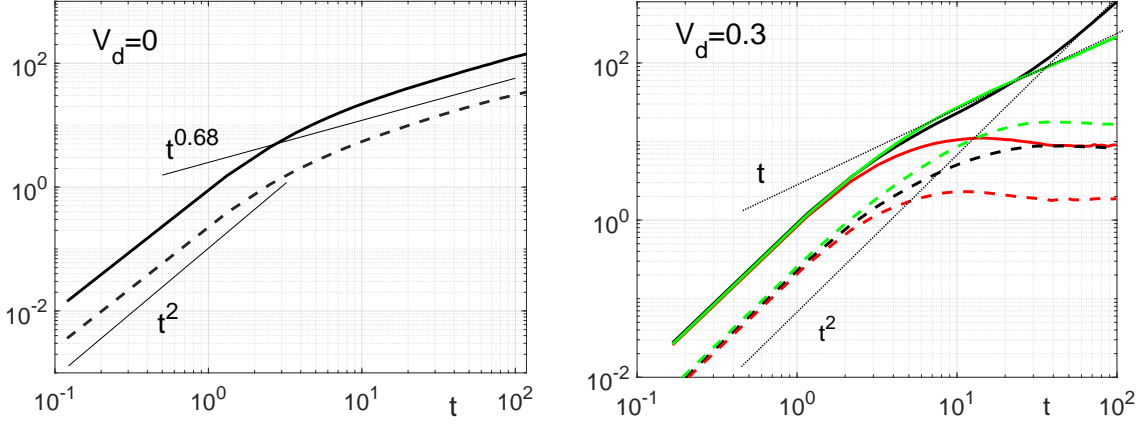


FIG. 10: The dispersions of the trajectories on the whole statistical ensemble (black line) for $V_d = 0$ (left panel) and $V_d = 0.2$ (right panel) as functions of time. The dashed lines are for $x_1(t)$ and the solid lines for $x_2(t)$. The conditional dispersions for trapped (red) and free (green) trajectories are also shown in the right panel.

The dispersions of the trajectories (Fig. 10) are connected to the correlations of the Lagrangian velocity (Fig. 8) and to the time dependent diffusion coefficients, defined by $2D_i(t) = d \langle (\delta x_i(t))^2 \rangle / dt$, by Taylor formulas [14]

$$D_i(t) = \int_0^t L_i(\tau) d\tau, \quad \langle (\delta x_i(t))^2 \rangle = 2 \int_0^t (t - \tau) L_i(\tau) d\tau. \quad (21)$$

Similar equations can be written for each category of trajectories (trapped or free). Figure 11 presents the time dependent diffusion coefficients compared to their restrictions to the trapped and free trajectories for the x_1 (left panel) and x_2 (right panel) directions. This confirms that the perpendicular diffusion is completely hindered (even for the free trajectories). The time integral of $L_1(t)$ vanishes for all categories at a finite time. The parallel transport is ballistic $D_2(t) \sim t$, in spite of the normal diffusion of the free trajectories and of the total confinement of the trapped ones. It is the result of the ordered parallel motion, as seen by performing the time derivative in Eq. (20).

The probability of the displacements $P(\mathbf{x}, t)$ is strongly non-Gaussian, as seen in in Fig. 12 (black curves). The contributions of the two categories of trajectories are completely different: the trapped trajectories determine the steep peak in $\mathbf{x} = \mathbf{0}$, and the free ones have a large Gaussian distribution with the average parallel displacement $\langle x_2(t) \rangle_{fr} = V_d t / n_{fr}$. We note that the transport, which is essentially produced by the free trajectories, results from a Gaussian distribution.

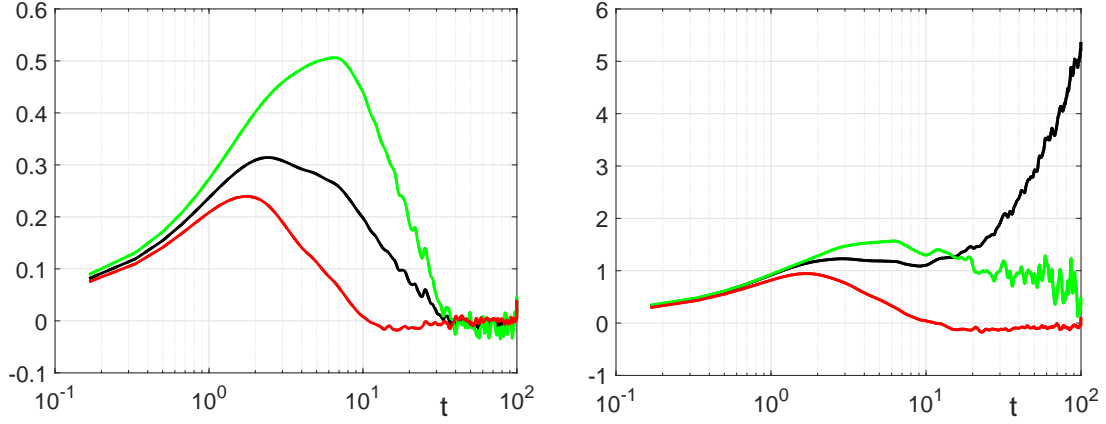


FIG. 11: The time dependent diffusion coefficients in the direction perpendicular (left panel) and parallel (right panel) to the average velocity for the whole statistical ensemble R (black lines) and restricted to the tr (red lines) and fr (green lines) subensembles. $V_d = 0.2$.

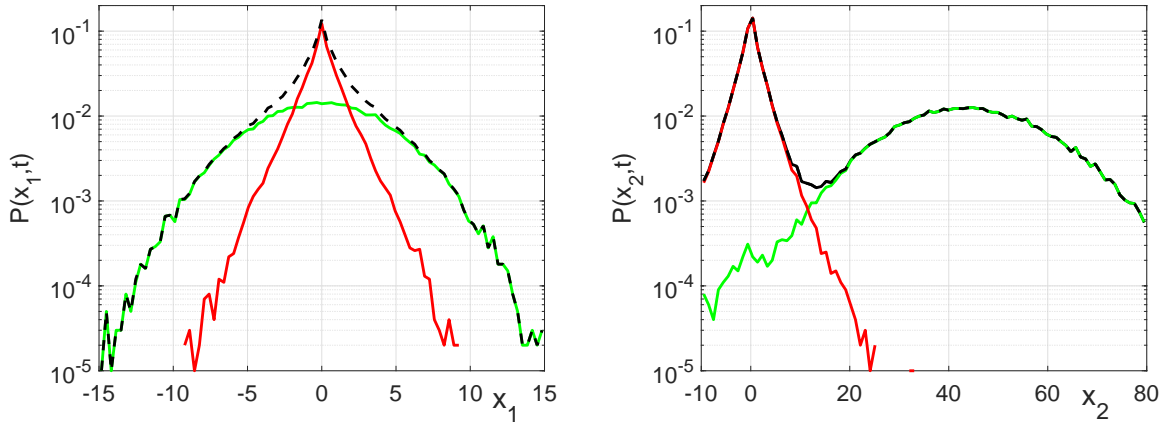


FIG. 12: The probabilities of the x_1 (left panel) and x_2 (right panel) for the whole set of realizations (black lines) compared to the contributions of the free (green lines) and trapped (red lines) trajectories for $V_d = 0.2$ and $t = 97$.

5. COHERENCE INDUCED BY AN AVERAGE VELOCITY

The Hamiltonian structure of equation (1) is the origin of the order that characterizes the two-dimensional incompressible turbulence. It determines the strong connection between trajectories and the contour lines of the potential, which are paths of the motion. The order (quasi-coherence) of the motion is essentially represented by the existence of correlations between the potential and the trajectories. They are represented by nonzero average displacements or velocities conditioned by the (initial) potential.

Significant quasi-coherent characteristics of the transport process can be found by analyzing statistical Lagrangian quantities restricted on the contour lines with given potential ϕ^0 . The trajectories that belong to this class correspond to solutions of Eq. (1) that start (in $\mathbf{x}(0) = \mathbf{0}$) from points with $\phi(\mathbf{0}) = \phi^0$. The invariance of the total potential in this class gives

$$\phi_t(\mathbf{x}(t)) = \phi(\mathbf{x}(t)) + x_1(t)V_d = \phi^0. \quad (22)$$

The fractions of trajectories that evolve on the ϕ^0 potential lines, the average and the amplitude of fluctuations of their displacements and Lagrangian velocities are determined below for each type of trajectories using conditional averages.

The analysis starts from the representation (9) and introduces a supplementary condition for the trajectories, namely that the initial potential is ϕ^0 [$\phi(\mathbf{x}(0)) = \phi^0$]. Defining the fraction of these trajectories by $n(\phi^0)$ and the

corresponding conditional average by $\langle \cdot \rangle_{\phi^0}$, the average $\langle A(\mathbf{x}(t)) \rangle$ is the sum of the contributions from each value ϕ^0

$$\langle A(\mathbf{x}(t)) \rangle = \int_{-\infty}^{\infty} \langle A(\mathbf{x}(t)) \rangle_{\phi^0} P(\phi^0) d\phi^0, \quad (23)$$

where $P(\phi^0)$ is the Gaussian distribution of the (normalized) potential

$$P(\phi^0) = \frac{1}{\sqrt{2\pi}} \exp\left(-\frac{(\phi^0)^2}{2}\right). \quad (24)$$

Similar equations can be written for the contributions of the free and trapped trajectories

$$n_c \langle A(\mathbf{x}(t)) \rangle_c = \int_{-\infty}^{\infty} \langle A(\mathbf{x}(t)) \rangle_{\phi^0,c} n^c(\phi^0) d\phi^0, \quad (25)$$

where $n^c(\phi^0)$ is the fraction of trajectories that evolve on contour lines ϕ^0 and are in the category $c = tr, fr$, and $\langle \cdot \rangle_{\phi^0,c}$ is the conditional average taken on the subensemble of these trajectories. $n^c(\phi^0)$ is related to n_{tr}, n_{fr} (defined in Section 3)

$$n_c = \int_{-\infty}^{\infty} n^c(\phi^0) d\phi^0. \quad (26)$$

One obtains using Eq. (9)

$$\langle A(\mathbf{x}(t)) \rangle_{\phi^0} P(\phi^0) = \langle A(\mathbf{x}(t)) \rangle_{\phi^0,tr} n^{tr}(\phi^0) + \langle A(\mathbf{x}(t)) \rangle_{\phi^0,fr} n^{fr}(\phi^0), \quad (27)$$

which connects the contribution of all trajectories $\langle A \rangle_{\phi^0} P(\phi^0)$ to the contributions of each category $\langle A \rangle_{\phi^0,c} n^c(\phi^0)$.

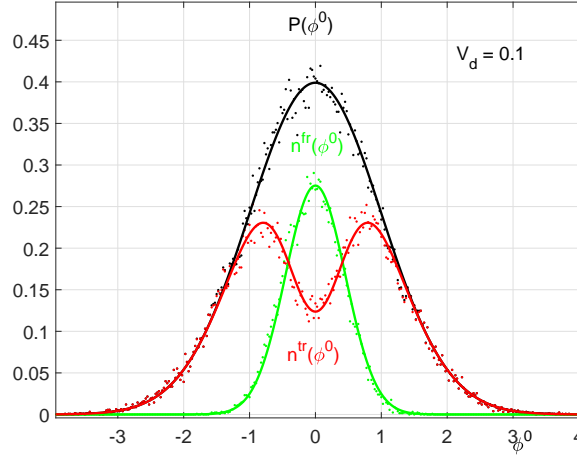


FIG. 13: The fraction of the trajectories that evolve on the contour lines with potential ϕ^0 for the free (green points), trapped (red points) and for all trajectories (black points) obtained from the numerical simulations compared to $P(\phi^0)$ (solid black line), with Eq. (29) (solid green line) and Eq. (31) (solid red line).

The fractions of trajectories fulfil the equation

$$P(\phi^0) = n^{tr}(\phi^0) + n^{fr}(\phi^0), \quad (28)$$

which is obtained from Eq. (27) for $A = 1$. The numerical results obtained for $n^{fr}(\phi^0)$ and $n^{tr}(\phi^0)$ (represented by points), are compared to analytical approximations (solid lines) in Fig. 13. One can see that the fraction of trajectories that evolve on ϕ^0 contour lines (black line and points in Fig. 13) reproduces Eq. (24). The fraction of the free trajectories is narrower, but it is still Gaussian. We have found, as seen in Fig. 13 (green curve), a good approximation of the data by

$$n^{fr}(\phi^0) = n_{fr} G(\phi^0; \Delta), \quad (29)$$

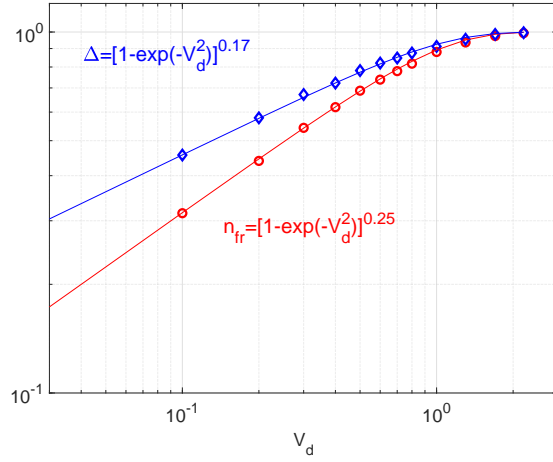


FIG. 14: The width Δ of the initial potential of the free trajectories (diamonds) and the fraction of free trajectories (circles) as functions of the average velocity V_d . The numerical results are interpolated by Eqs. (32) and (8)

where $G(\phi^0; \Delta)$ is the Gaussian distribution

$$G(\phi^0; \Delta) = \frac{1}{\sqrt{2\pi}\Delta} \exp\left(-\frac{(\phi^0)^2}{2\Delta^2}\right) \quad (30)$$

with a width Δ that depends on the average velocity V_d . The fraction of the trapped trajectories (red curve in Fig. 13), which according to Eq. (28) is

$$n^{tr}(\phi^0) = P(\phi^0) - n_{fr} G(\phi^0; \Delta), \quad (31)$$

provides a good representation of the numerical results (red points).

The width Δ as function of the average velocity V_d is shown in Fig. 14 together with the fraction of free trajectories n_{fr} . The numerical results for $\Delta(V_d)$ (diamonds) are well approximated by

$$\Delta(V_d) = [1 - \exp(-V_d^2)]^{0.17}. \quad (32)$$

Both functions saturate at large V_d ($V_d > V_1, V_2$), and they have power law dependence for small V_d

$$n_{fr} \sim V_d^{0.5}, \quad \Delta \sim V_d^{0.34}. \quad (33)$$

The asymptotic value $n_{fr} \rightarrow 1$ for $V_d \rightarrow \infty$ corresponds to the complete elimination of the islands of close contour lines of the potential ($n_{tr} = 0$). The limit $\Delta \rightarrow 1$ confirms that all trajectories are free, because $G(\phi^0; 1) = P(\phi^0)$, where $P(\phi^0)$ is the probability of the Eulerian potential.

Thus, the free trajectories are localized on the contour lines with small values of $|\phi^0| \lesssim \Delta$. The potential on the geometrical locus of free trajectories is Gaussian with an amplitude that is smaller than in the whole space.

The trapped (periodic) trajectories mainly have large $|\phi^0|$: they completely occupy the range of large potential $|\phi^0| \gg \Delta$, but also have significant presence at small potential $|\phi^0| \lesssim \Delta$ that correspond to free trajectories.

The average displacements conditioned by the value of the initial potential and by the category of the trajectories are shown in Fig. 15 for free (green), trapped (red) and all (black) trajectories. The perpendicular (left panel) and the parallel (right panel) displacements are shown at a large time $t = 97$, larger than the saturation time of $n_{fr}(t, V_d)$ (seen in Fig. 5, left panel). These represent quasi-coherent components of the motion, and appear only in the presence of an average velocity. One can see that the average conditional displacements are small for the trapped trajectories (red points), and that significant values appear for the free trajectories in both directions (green points). As shown in Fig. 15, these quantities can be approximated by

$$\langle x_1(t) \rangle_{\phi^0, fr} = \frac{\phi^0}{V_d}, \quad \langle x_1(t) \rangle_{\phi^0, tr} \cong 0, \quad (34)$$

$$\langle x_2(t) \rangle_{\phi^0, fr} = \frac{V_d t}{n_{fr}}, \quad \langle x_2(t) \rangle_{\phi^0, tr} = 0, \quad (35)$$

which are represented by red and green lines respectively. The black lines have the equations

$$\langle x_1(t) \rangle_{\phi^0} = \frac{\phi^0}{V_d} F(\phi^0), \quad \langle x_2(t) \rangle_{\phi^0} = \frac{V_d t}{n_{fr}} F(\phi^0), \quad (36)$$

where

$$F(\phi^0) = \frac{n^{fr}(\phi^0)}{P(\phi^0)} = \frac{n_{fr}}{\Delta} \exp\left(-\frac{(\phi^0)^2}{2} \frac{1 - \Delta^2}{\Delta^2}\right). \quad (37)$$

They result from Eq. (27) with $A = x_i(t)$ using (34) and (35), and provide, as seen in Fig. 15, good approximations of the data for $\langle x_i(t) \rangle_{\phi^0}$ (black points).

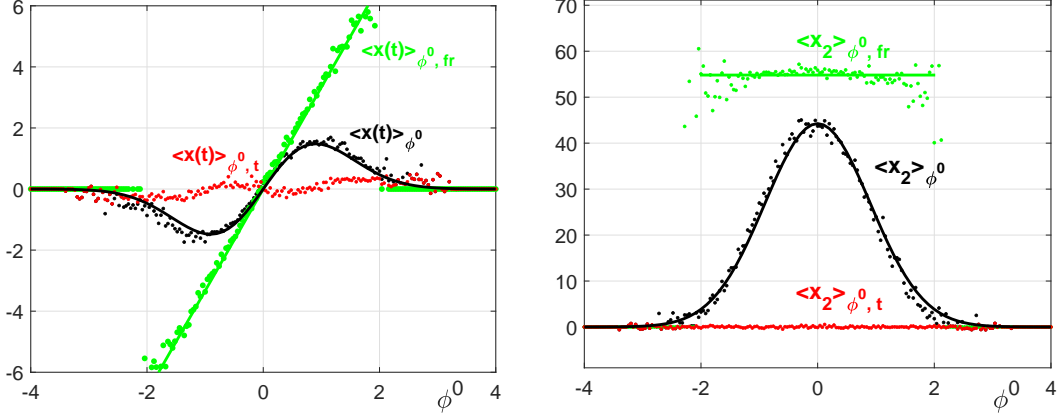


FIG. 15: The conditional average displacements along x_1 axis (left panel) and along x_2 axis (right panel) as functions of ϕ^0 for the trapped (red points), free (green points) and all (black points) trajectories, compared to the approximations (34)-(35) (green lines) and (36) (black lines). $V_d = 0.3$.

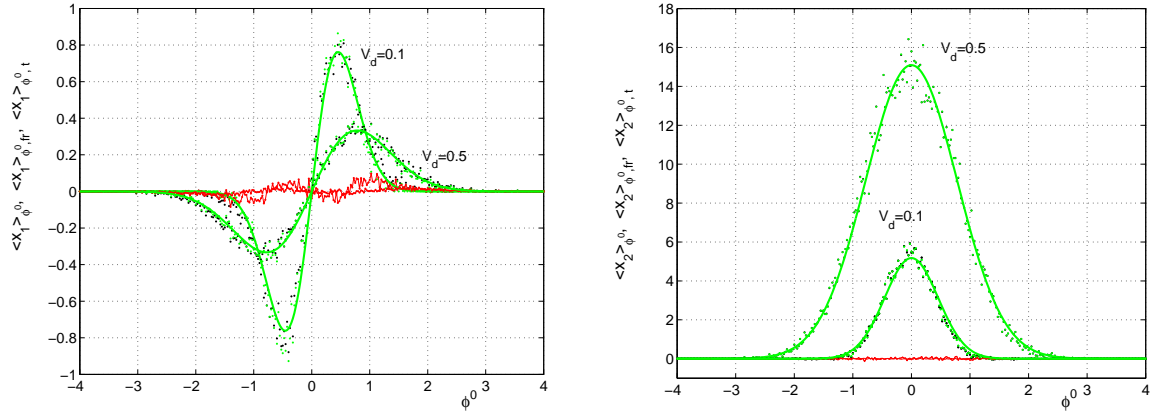


FIG. 16: The contributions of the trapped (red points) and free (green points) trajectories, to the average displacements (black points) along x_1 (left panel) and x_2 (right panel) directions as functions of ϕ^0 for the values of V_d label the curves. The approximations for the free trajectories are represented by the green lines.

The contributions to the average displacements, obtained by multiplying the conditional averages with the corresponding fractions of trajectories ($P(\phi^0)$, $n^{fr}(\phi^0)$ or $n^{tr}(\phi^0)$), are shown in Fig. 16. It appears more clearly that the coherent displacements are produced only by the free trajectories. The black points for all trajectories are practically superposed on the green points and they are well approximated by the green lines that represent the contributions of

the free trajectories ($\phi^0/V_d n^{fr}(\phi^0)$ in the left panel and $V_d t/n_{fr} n^{fr}(\phi^0)$ in the right panel). The dependence on ϕ^0 is different across and along the average velocity \mathbf{V}_d . In the first case, it is an anti-symmetrical function of ϕ^0 that saturates in time, and, in the second case, it is a symmetrical Gaussian function that increases linearly in time.

The parallel average displacement on the contour lines with initial potential ϕ^0 , which increases linearly with t (35), leads to an average Lagrangian velocity

$$\langle v_2(t) \rangle_{\phi^0, fr} = \frac{V_d}{n_{fr}}. \quad (38)$$

It is important to note that this velocity does not depend on ϕ^0 , and it equals the average velocity (10). The contribution of the conditional average velocity is determined only by the free trajectories since $\langle v_2(t) \rangle_{\phi^0, tr} = 0$. The perpendicular average displacement of the free trajectories also determines an average velocity, but it is transitory since $\langle x_1(t) \rangle_{\phi^0, fr}$ saturates in time.

The dispersion of the trajectories conditioned by the value of the initial potential and by the category are shown in Fig. 17 for free (green), trapped (red) and all (black) trajectories, in the perpendicular (left panel) and parallel (right panel) directions. One can see that the dispersion of the free trajectories along both directions are not dependent on the initial potential ϕ^0 , and can be approximated by

$$\langle \delta x_1^2 \rangle_{\phi^0, fr} = \frac{\Delta^2}{V_d^2}, \quad \langle \delta x_2^2 \rangle_{\phi^0, fr} = 2 D_2^{fr} t \quad (39)$$

represented by the green lines. On the contrary, the trapped trajectories have dispersions that decay with the increase of ϕ^0 (the red points). The dispersion of the trajectories conditioned by the potential is obtained using Eq. (27) for $A = x_i^2(t)$

$$\langle \delta x_i^2 \rangle_{\phi^0} = \langle \delta x_1^2 \rangle_{\phi^0, fr} F + \langle \delta x_1^2 \rangle_{\phi^0, tr} (1 - F) + \langle x_i(t) \rangle_{\phi^0, fr}^2 F(1 - F), \quad (40)$$

which depends on ϕ^0 as seen in Fig. 17 (black points).

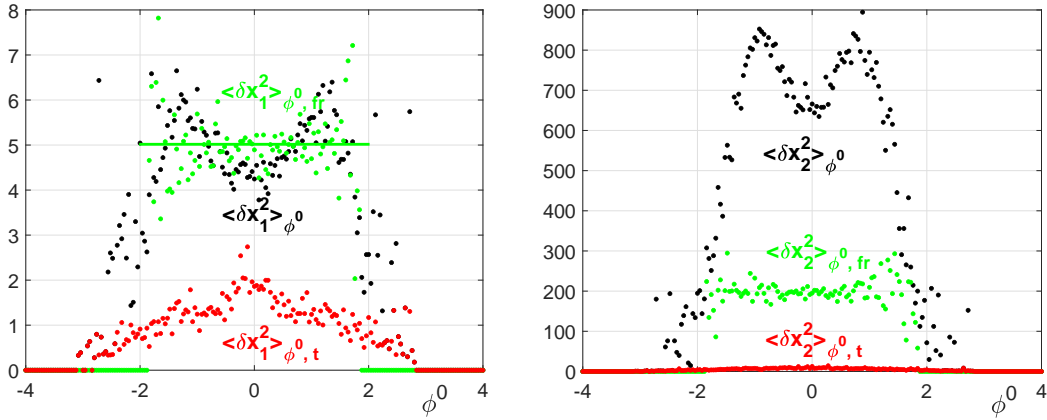


FIG. 17: The conditional trajectory dispersion along x_1 axis (left panel) and along x_2 axis (right panel) as functions of ϕ^0 for the trapped (red points), free (green points) and all (black points) trajectories, compared to the approximations (39) (green lines). $V_d = 0.3$ and $t = 97$.

Thus, the analysis of the Lagrangian statistics conditioned by the initial potential reveals a coherent component of motion perpendicular to \mathbf{V}_d . It consists of average displacements that have the sign correlated with the sign of ϕ^0 . They appear for the free trajectories and are hidden in the sense that the contributions of all contour lines (with all values of ϕ^0) mix to zero. The amplitude of the ordered motion is defined by the displacements conditioned by the sign of ϕ^0 , $\langle x_1(t) \rangle_+$ obtained by integration over ϕ^0 on the interval $[0, \infty)$ and $\langle x_1(t) \rangle_-$ that is the integral over $(-\infty, 0]$. These are symmetrical quantities since $\langle x_1(t) \rangle = \langle x_1(t) \rangle_+ + \langle x_1(t) \rangle_- = 0$. The time derivatives of these functions determine a pair of average velocities with opposite directions that exactly compensate each other (the hidden drifts, HDs) that are oriented across \mathbf{V}_d . The HDs were first found in [15] using an approximate theoretical approach, the decorrelation trajectory method [16]. In the presence of components of the motion that introduce a

small compressibility, an average velocity can be generated by breaking the equilibrium of the HDs. Such effects were found in magnetically confined plasmas [17]-[19]. The HDs are transitory in frozen potentials because the average displacements saturate $\langle x_1(t) \rangle_{\phi^0, fr} \rightarrow \phi^0/V_d$.

The analysis also shows that the parallel motion is similar on the contour lines with different ϕ^0 , and that it depends only on the category of trajectories. The asymptotic value $\langle x_1(t) \rangle_{\phi^0, fr} \rightarrow \phi^0/V_d$ represents the centrum of the space domain that contains the trajectories, which start from points on the line $x_1 = 0$ where the potential is ϕ^0 . It is limited by the lines $x_1^- = (\phi^0 - \Delta)/V_d$, $x_1^+ = (\phi^0 + \Delta)/V_d$, and has infinite dimension along \mathbf{V}_d . Reported at this centrum, the free trajectories are statistically identical for all values of the initial potential ϕ^0 .

6. LAGRANGIAN STATISTICS IN TIME DEPENDENT POTENTIALS

The general conclusion of the analysis of trajectory statistics in frozen potentials is the existence of a high degree of coherence, which reflects the structure of the contour lines of $\phi_t(\mathbf{x})$ on which the trajectories are bounded.

The time-dependence of the potential determines the variation of the Lagrangian potential and the decorrelation from its initial value ϕ^0 . It is expected to strengthen the random aspects of the trajectories and to cause the elimination of the Lagrangian coherence in a time of the order of the decorrelation time τ_c . More precisely, the random time-variation of the potential should vanish the averages and correlations conditioned by ϕ^0 , which show the existence of hidden order. It is thus expected that the order found in static potential is in this case only a transitory processes with life-time τ_c .

The trajectories are more complex than in static potentials. Closed periodic trajectories do not exist in time dependent potentials, but trapping events represented by almost closed eddying segments appear on all trajectories when the decorrelation time τ_c is large compared to the time of flight $\tau_{fl} = \lambda/V$, ($\lambda = (\lambda_1^2 + \lambda_2^2)^{1/2}$ and $V = (V_1^2 + V_2^2)^{1/2}$), and the integration time is much longer than τ_c . The trapping events are separated by long jumps, which are similar with the free trajectories.

The separation of the trajectories in the categories $c = tr, fr$ has no meaning in time-dependent potentials. However one can define related quantities that are not properties of the trajectories but of the contour lines of the potential. The latter are geometric objects. The fraction of free/trapped trajectories can be defined using the number of trajectories that stay on open/closed contour lines of the potential at time t . These fractions do not depend on time for stationary stochastic potentials, because the amplitude, the space correlation and the structure of the contour lines are statistically time-invariant. They equal the asymptotic values of the time dependent fractions $n_c(t, V_d)$ obtained in static potentials from the trajectories (Sections 3)

$$n_c(V_d) = \lim_{t \rightarrow \infty} n_c(t, V_d), \quad (41)$$

for any τ_c and $c = tr, fr$. In a similar way, the fraction of trajectories that stay at time t on contour lines of category c with the potential $\phi^t = \phi(\mathbf{x}(t))$ is a time-independent function of ϕ^t and c , which is the asymptotic value $n^c(\phi^t)$ of the fractions obtained in static potential ($\tau_c \rightarrow \infty$) in Eqs. (29-31). The physical meaning of these quantities will be clarified after analyzing the significant modifications of the statistics of trajectories produced by the time-variation of the potential.

We underline that, in time-dependent potentials, one can define the statistics conditioned by the initial potential, but not by the category.

Our aim is to see if the special order determined by the average velocity survives at finite τ_c . We analyze here the statistics on the whole set of trajectories (in R), while, in the next section, the statistics conditioned by the initial potential will be used for understanding the direct effects of time variation on the coherent elements found here.

The time variation of ϕ represents a decorrelation mechanism, because it determines the stochastic change of the Lagrangian velocity, which vanishes the Lagrangian correlations $L_i(t)$ at times $t \gg \tau_c$. Usually, this produces the saturation of the time dependent diffusion coefficients $D_i(t) \rightarrow D^i$ and diffusive transport with $\langle \delta x_i^2(t) \rangle \rightarrow 2D^i t$ (as obtained from Eq. (21)). The memory of the initial velocity is lost in a time τ_c , which means that the displacements at large time $t \gg \tau_c$ are sequences of non-correlated random steps that yield a Gaussian distribution.

We show that this general behavior is not at all observed in the presence of \mathbf{V}_d at large correlation times (weak time variation). A strong non-standard influence appears both on the transport and on the probability of the displacements.

The Lagrangian velocity is, as expected, Gaussian at any time and for any τ_c , as in the static case. The time variation influences only its correlation.

The dispersions of the trajectories $\langle \delta x_i^2(t) \rangle$ and the probabilities $P(x_i, t)$ for a typical case that illustrates the effects of weak time variation of the potential are shown in Figs. 18 and 19, by the black lines for $V_d = 0.3$ and $\tau_c = 33$. We also present, for comparison, two examples with $V_d = 0.3$ (for the static case $\tau_c = \infty$ (red lines) and for fast time variation $\tau_c = 3.3$ (blue)), and two examples with $V_d = 0$ (for $\tau_c = \infty$ (green) and $\tau_c = 33$ (cyan)).

When $V_d = 0$, the subdiffusive transport at $\tau_c = \infty$ with $\langle \delta x_i^2(t) \rangle \sim t^{0.68}$ is transformed into normal transport ($\langle \delta x_i^2(t) \rangle \rightarrow 2D^i t$) at large τ_c (Fig. 18, green and cyan curves). The process appears for all finite values of τ_c , which only influence the diffusion coefficients D^i . However, the probabilities of displacements are Gaussian only for fast time variation. In the static case, $P(x_i, t)$ has a steep peak in $x_i = 0$, which corresponds to trapped trajectories, superposed on a large Gaussian component, which yields from the trajectories that are not closed at time t . The steep peak is flattened by time variation and the probabilities have extended exponential shapes at large τ_c . When τ_c decreases, $P(x_i, t)$ evolves to Gaussian distribution, which is attained when $\tau_c < \tau_{fl}$.

The average velocity makes the transport strongly anisotropic. In frozen potential $\tau_c = \infty$, the transport is ballistic in the parallel direction and saturated perpendicular to \mathbf{V}_d , as discussed in Section 4.2 and also shown in Figs. 18 and 19 (red curves). The normal transport and the Gaussian probability are reached only for fast time variation of the potential ($\tau_c < \tau_{fl}$), as seen in the example for $\tau_c = 3.3$ (blue curves). In these conditions, the motion along the contour lines of $\phi(\mathbf{x}, t)$ is completely hindered, which means that the quasi-coherent components are eliminated.

Compared to these cases, the trajectory statistics at slow time variation in the presence of V_d (the black curves) is strongly anomalous with complex behavior. Trajectory dispersion at large time has nonstandard time-dependence in both directions

$$\langle \delta x_1^2(t) \rangle \sim t^{\alpha_1}, \quad \langle \delta x_2^2(t) \rangle \sim t^{\alpha_2},$$

where $\alpha_1 < 1$ and $\alpha_2 > 1$, which corresponds to subdiffusive perpendicular transport (but not saturated as in the static case) and superdiffusive parallel transport (but not of ballistic type). These powers are functions of τ_c and V_d , $\alpha_i(\tau_c, V_d)$. When τ_c decreases, α_1 increases and saturates $\alpha_1 \rightarrow 1$, while α_2 decreases and saturates $\alpha_2 \rightarrow 1$. A similar effect is determined by the increase of V_d , which leads to normal transport at $V_d \gtrsim 1$. In the example presented in Fig. 18 (black curves), $\alpha_1(33, 0.3) = 0.57$, $\alpha_2(33, 0.3) = 1.35$. The probabilities are very large, especially in the parallel direction, and the peak in $\mathbf{x} = 0$ persists for very long time ($t = 300 = 6\tau_c$ in Fig. 19).

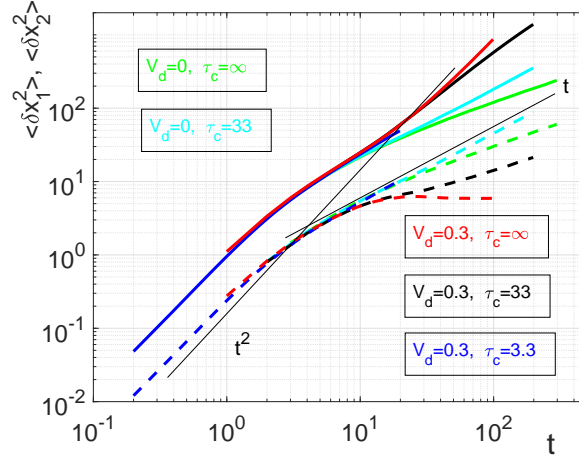


FIG. 18: Comparison of the dispersions of the trajectories in time-dependent potential with the static cases along x_1 (dashed lines) and x_2 (solid lines) directions. The values of V_d and τ_c label the curves.

Thus, the transport and the statistics of displacements are non-standard when $V_d \lesssim 1$ and $\tau_c > \tau_{fl}$. In these conditions the structure of the contour lines of the potential shows island of closed lines in a network of open lines. Also, the trajectories approximately follow the contour lines for distances of the order of the correlation length before they are removed by the time variation of the potential.

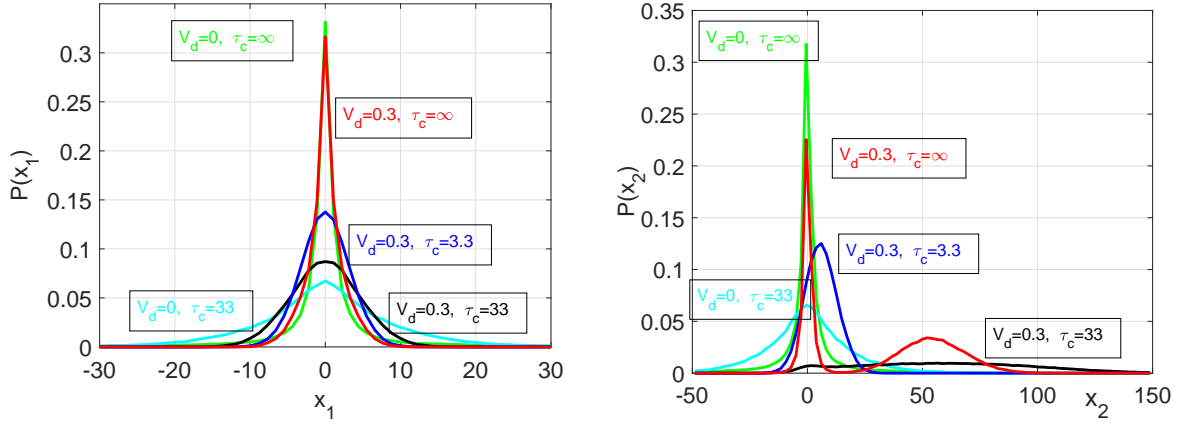


FIG. 19: The probabilities of the displacement along x_1 (left panel) and x_2 (right panel) directions, show the effect of the time variation of the potential for typical cases with the values of V_d and τ_c that label the curves.

7. ENHANCED COHERENCE AND LONG MEMORY EFFECTS

7.1 Hidden ordered motion

Ordered motion conditioned by the initial potential ϕ^0 was found in the presence of an average velocity V_d for the free trajectories. It is represented by the average displacements $\langle x_i(t) \rangle_{\phi^0, fr}$ that are conditioned by the initial potential and by the category $c = fr$ [Eq. (36)]. These quantities obtained in a time-dependent potential (with $\tau_c = 33$) are shown in Fig. (20) for x_1 and in Fig. (21) for x_2 , compared to the static case. Significant differences appear for both directions.

One can see in Fig. (20, left panel) that the perpendicular displacements $\langle x_1(t) \rangle_{\phi^0}$ are larger in time-dependent potential, although the calculations are at a very large time, $t = 6\tau_c$ (where the EC of the potential (3) is negligible, $E(t) = 10^{-8}$). The main contribution comes from large values of the potential $|\phi^0|$, which is negligible in the static potential. The amplitude of the ordered motion is represented by the average displacements conditioned by the sign of ϕ^0 , $\langle x_1(t) \rangle_+$ and $\langle x_1(t) \rangle_-$, which determine by time derivative the HDs. Surprisingly, the time evolution of these quantities shows a continuous increase in time-dependent potential, while it saturates in the static case, as seen in Fig. (20, right panel) for $\langle x_1(t) \rangle_+$. This means that the hidden drifts are transitory in static potentials, but they are long-life statistical quantities in time dependent potential. Their amplitude decays on a long time scale, much longer than the decorrelation time of the potential.

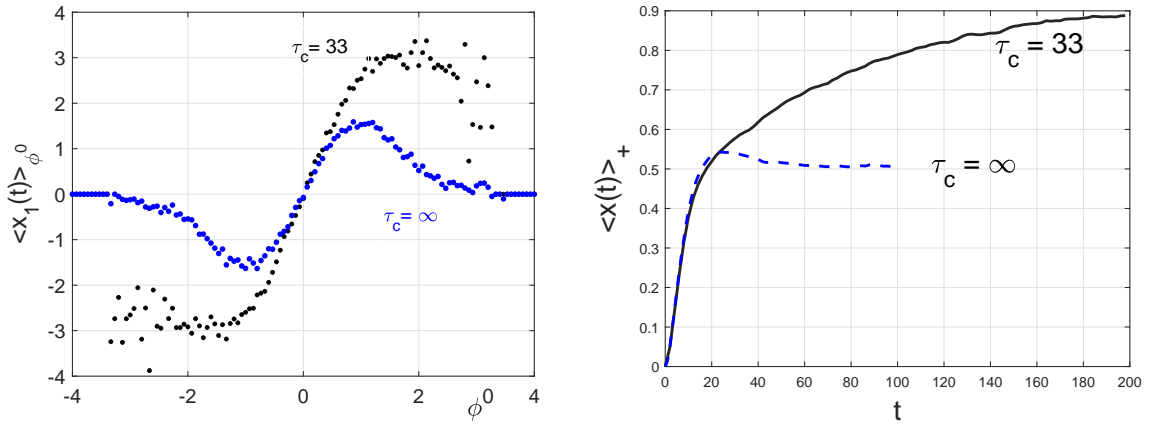


FIG. 20: Ordered perpendicular displacements $\langle x_1(t) \rangle_{\phi^0}$ as functions of ϕ^0 at $t = 200$ (left panel) and $\langle x_1(t) \rangle_+$ as function of time (right panel) for a time-dependent potential with $\tau_c = 33$ (black points) compared to the static case (dashed blue lines)

The time variation of the potential modifies the parallel displacements $\langle x_2(t) \rangle_{\phi^0}$ by determining the extension of

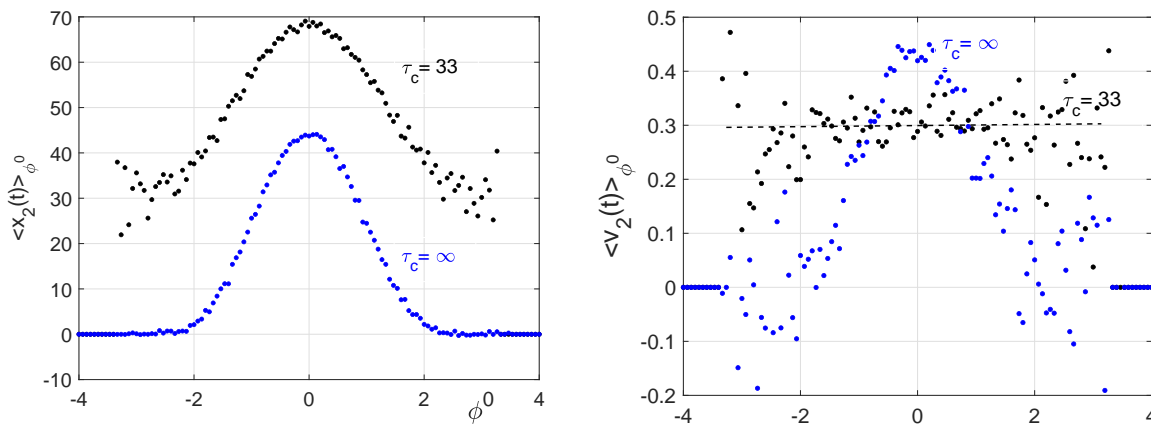


FIG. 21: Ordered parallel displacements $\langle x_2(t) \rangle_{\phi^0}$ (left panel) and average velocity $\langle v_2(t) \rangle_{\phi^0}$ (right panel) as functions of ϕ^0 at $t = 200$ for a time-dependent potential with $\tau_c = 33$ (black points) compared to the static case (dashed blue lines)

the contribution on the whole range of ϕ^0 and the dependence on these quantities of the initial potential (Fig. (21, left panel). It is peaked on $\phi^0 = 0$ and has a weak (algebraic) decay at large $|\phi^0|$, instead of the concentration on the domain of free trajectories with uniform average displacement Eq. (35). However, the average Lagrangian velocity is uniform on the whole range of ϕ^0 and it has the Eulerian value V_d , as seen in Fig. (21, right panel). The process of concentration of the Lagrangian average velocity on the domain of free trajectories found in static potentials is eliminated by the time-variation.

The fluctuations of the trajectories $\langle \delta x_i^2(t) \rangle_{\phi^0}$ and the transport $\langle \delta x_i(t) \delta v_i(t) \rangle_{\phi^0}$ conditioned by the initial potential are all asymptotically uniform on the whole domain of ϕ^0 . They reach this stage in a long time compared to the correlation time of the potential ($t \gg \tau_c$) starting from the values corresponding to static potential that are maintained at small time $t < \tau_c$.

These results show that the trajectories are statistically identical with the exception of the perpendicular average displacement $\langle x_i(t) \rangle_{\phi^0}$, which depend on ϕ^0 .

7.2 Long memory

The persistent Lagrangian order and the non-standard characteristics of the trajectories in the time dependent case can be understood by analyzing the statistics of the Lagrangian potential $\phi(t) \equiv \phi(\mathbf{x}(t), t)$.

The distribution of the Lagrangian potential has the same invariance property as the Lagrangian velocity. It has the Gaussian probability of the Eulerian potential at any time t , for both the static and the time-dependent cases, at any value of the average velocity V_d . However, significant differences appear between these cases concerning the correlation and the average conditioned by the initial potential, as seen in Figs. (22) and 23.

The correlation of the Lagrangian potential $L_\phi(t) = \langle \phi(0) \phi(t) \rangle$ is far from the Eulerian time-correlation, $E(\mathbf{0}, t)$. Starting from the trivial case of static potential with $V_d = 0$, where the invariance of the potential implies $L_\phi(t) = E(\mathbf{0}) = 1$, in all the other cases shown in Fig. (22), the Lagrangian correlation is stronger than the Eulerian one, as it has a long tail with much slower decay. It demonstrates that the Lagrangian potential has a long-time memory.

The memory effect is strongest in almost static potentials (very large τ_c) with average velocity $V_d = 0$. The Lagrangian correlation decreases much slower than the Eulerian one, and it is larger than than $E(\mathbf{0}, t)$ at any time (Fig. 22, the curve for $V_d = 0$, $\tau_c = 33$). In this example, at $t = 200 \cong 6\tau_c$, L_ϕ decreases only at 0.4, while $E(\mathbf{0}, t) = 1.5 \cdot 10^{-8}$.

The average velocity ($V_d \neq 0$) determines a faster decrease of $L_\phi(t)$ at small time that leads to smaller values compared to the case $V_d = 0$ (Fig. 22, the curve for $V_d = 0.3$, $\tau_c = 33$). The decorrelation takes place on two time-scales. There is a fast decay at small time that is followed by a slow decrease of $L_\phi(t)$. The fast decay is the same for $\tau_c = \infty$ and $\tau_c = 33$ at $V_d = 0.3$, which shows that this process is not a consequence of the potential time variation, but rather of the presence of V_d .

In the static case, the memory of the Lagrangian potential is infinite ($L_\phi(t)$ saturates). The asymptotic value is positive and it is a decreasing function of V_d . The time-dependence of $L_\phi(t)$ is the result of a selective decorrelation mechanism determined by the average velocity. This process can be understood by analyzing the correlation of $\phi(t)$

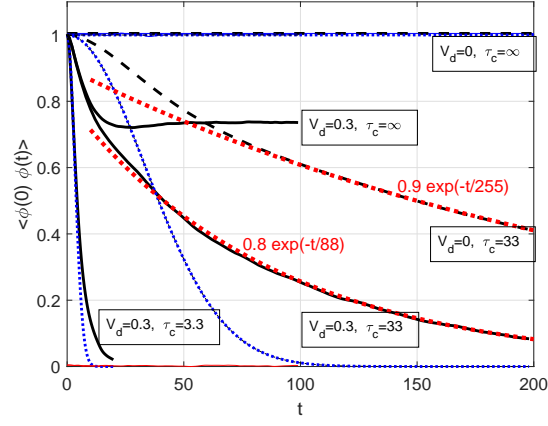


FIG. 22: Correlation of the Lagrangian potential for $V_d = 0$ (dashed lines) and $V_d = 0.3$ (continuous lines) for static ($\tau_c = \infty$), slow ($\tau_c = 33$) and fast time-variation ($\tau_c = 3.3$), compared to the Eulerian correlations (dotted blue lines). Long tails with exponential decay appear in time-dependent potentials with large τ_c .

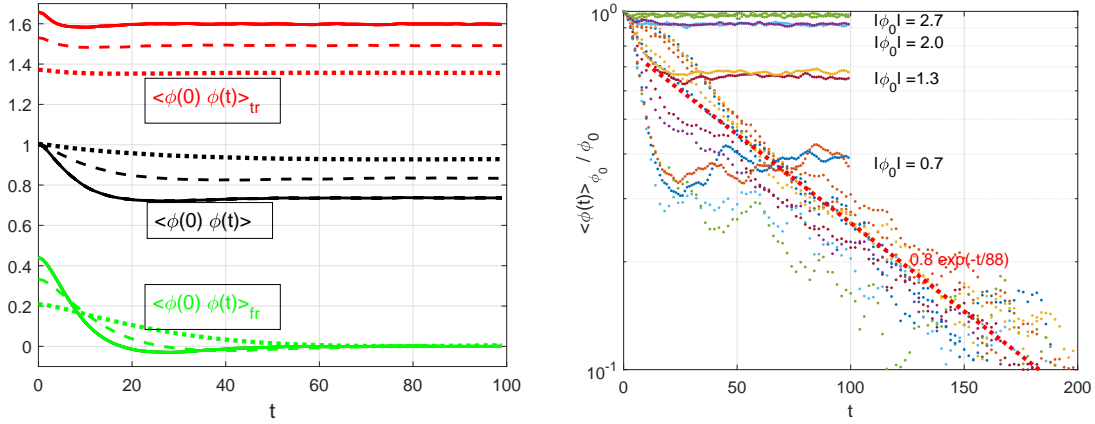


FIG. 23: Characterization of the memory of the Lagrangian potential. Left: The correlations conditioned by the category $\langle \phi(0) \phi(t) \rangle_c$ for $V_d = 0.1$ (dotted), $V_d = 0.2$ (dashed), $V_d = 0.3$ (continuous). Right: The normalized average potential conditioned by the initial potential for $V_d = 0.3$, for $\tau_c = \infty$ (continuous), $\tau_c = 33$ (dotted), and the values of ϕ_0 that label the curves.

conditioned by the category $c = tr, fr$ in the static potential ($\tau_c = \infty$). As seen in Fig. 23, left panel, $\langle \phi(0) \phi(t) \rangle_c$ decays to zero for the free trajectories, while it saturates for the trapped trajectories at a value that is comparable to the conditioned amplitude $\langle \phi^2(0) \rangle_{tr}$. This demonstrates that in static potential the decorrelation affects only the free trajectories and that the memory effect is determined by the trapped trajectories, which approximately maintain the initial potential $\phi(0)$. The asymptotic value of the average Lagrangian potential is thus

$$\langle \phi(0) \phi(t) \rangle = \langle \phi(0) \phi(t) \rangle_{tr} n_{tr} = \phi^0 n_{tr}. \quad (42)$$

It is interesting to note that at finite τ_c , the significant decrease of the correction appears at any time, although it seems that the process determined by V_d is transitory in static potentials. This is caused by the interaction of the effects of V_d with the influence produced by the time variation, which determine the two time-scale evolution of $L_\phi(t)$. It is clearly evidenced by the average Lagrangian potential conditioned by the initial value ϕ^0 normalized by this value, $\langle \phi(t) \rangle_{\phi_0} / \phi_0$ represented in Fig. 23, right panel for the static case (lines) and for $\tau_c = 33$ (points) for several values of ϕ_0 .

An important property of the Lagrangian potential in slow time-dependent potential is that its correlation and the average conditioned by ϕ^0 have the same time-decay (as seen in Fig. 22 for the case $V_d = 0.3, \tau_c = 33$ and in the right panel of Fig. 23, all the curves have the same behavior $\exp(-t/88)$).

The long memory of the potential and the increase of the average displacements $\langle x_1(t) \rangle_{\phi^0}$ (Fig. 20) are the result of the same process. It consists of the liberation of the trapped trajectories with large $|\phi^0|$ followed by repeated

stochastic events of capture and release combined with the constraint of the total potential invariance (22) that approximately holds for small time intervals. Considering the case of the peaks of the potential, the liberation of the trapped trajectories with large ϕ^0 is produced when the time variation determines the decrease of the potential to Δ . The contour lines of the potential that are open have the average perpendicular displacement Δ/V_d and the average potential along them equal to zero (as imposed by Eq. (22)). The stochastic recapture is uniformly distributed over the potential and has the average perpendicular location Δ/V_d . This cancels asymptotically the average of the potentials on the trapping events and leads to the average Δ/V_d of the positions of the trapping events. This happens on a time scale that is much larger than τ_c . These released trajectories with large ϕ^0 determine the slow decay of their initial average potential and the increase of their average displacement from zero to the largest possible value Δ/V_d . Thus, the memory of the Lagrangian potential and the strengthening of the coherence of the trajectories are both determined by the slow evolution toward uniform distribution of the trapping events on the trajectories caused by the time-variation of the potential.

8. SUMMARY AND CONCLUSIONS

A detailed study of the Lagrangian coherence of the trajectories in 2-dimensional incompressible velocity fields is presented. The strong order that appear in this kind of velocity fields is determined by the Hamiltonian structure of the advection equations (1), (2) and by the space correlation of the stochastic potential. The trajectories follow the contour lines of the potential in the static case, and, for slowly varying potentials, they remain close to them for long time intervals. This study is focused on the identification and understanding of the order generated by an average velocity V_d superposed on the stochastic field. It determines an average potential, which strongly modifies the structure of contour lines of the total potential $\phi_t(\mathbf{x}, t) = \phi(\mathbf{x}, t) + x_1 V_d$ by generation of a network of open lines between islands of closed lines. As a result, two categories of trajectories are found in static (frozen) potential: trapped (closed, periodic) and free (with unlimited displacement in the parallel direction to \mathbf{V}_d).

The results presented here are based on the numerical simulation of the trajectories and on a complex statistical analysis that includes conditional averages and correlations connected to the topology of the contour lines of the potential ϕ_t . The statistics of displacements and of the Lagrangian velocity are determined for the whole ensemble R , for the categories trapped (*tr*) and free (*fr*), and also on sets of contour lines of the potential conditioned by the value ϕ^0 at the starting point of the trajectories. This analysis reveals the origin of coherence and provides explanations for the nonstandard statistics, transport and memory of this motion.

In the case of frozen potentials, we have found that the statistical properties determined for the two categories *tr*, *fr* are completely different compared to those obtained in the whole space R . The average velocity V_d generates coherence in the Lagrangian velocity, which acquires average components from the stochastic ones for both categories. The supplementary coherent velocity cancels the average velocity V_d of the trapped trajectories, and it determines larger velocity for the free trajectories that compensate the missing contribution of the trapped ones ($\langle v_2(t) \rangle_{fr} = V_d/n_{fr}$). Thus, the statistical invariance of the Lagrangian velocity (Lumley theorem) is ensured in a rather non-trivial manner that involves hidden coherent parallel velocity.

The statistical analysis conditioned by the initial potential ϕ^0 reveals additional important aspects. The free trajectories have Gaussian distribution of ϕ^0 with a width Δ that is smaller than the dispersion of the Eulerian potential. It shows the existence of ordered perpendicular motion (average displacements across \mathbf{V}_d (34)) that appear for the free trajectories and are proportional with ϕ^0 . These averages $\langle x_1(t) \rangle_{\phi^0, fr}$ increase in time from zero and saturate at ϕ^0/V_d . They generate the hidden drifts, a pair of transitory average velocities perpendicular on \mathbf{V}_d conditioned by the sign of ϕ^0 , which have opposite directions and exactly compensate each other. We have also found that the Lagrangian statistics of the free trajectories conditioned by ϕ^0 depends on the value ϕ^0 only through the average perpendicular displacement. This means that the trajectories in the category *fr* for different values of ϕ^0 are statistically identical, and are organized in strips with limited perpendicular extensions.

The probability of the displacements is non-Gaussian with separated contributions of the categories: a steep peak for *tr* and Gaussian distribution that move along \mathbf{V}_d , but with larger velocity V_d/n_{fr} for the *fr* subensemble. The time-invariant Gaussian distribution of the Lagrangian velocity is the sum of the non-Gaussian contributions of the two categories, which are both non-Gaussian, but invariant.

The transport is produced only by the free trajectories. A paradoxical behavior was found: the statistics of the trajectories is strongly non-Gaussian, but the transport is produced by Gaussian trajectories, which in fact yield from the non-Gaussian velocity distribution of the free trajectories. The transport is anomalous, subdiffusive across \mathbf{V}_d and superdiffusive of ballistic type along \mathbf{V}_d . The latter results from the ordered parallel motion. category.

The free trajectories can be associated to a geometrical locus on the two-dimensional space (x_1, x_2) , in the sense

that each point is the initial condition for such trajectory and all trajectories are confined in this domain fr . The complement of fr is the geometric locus of the trapped trajectories tr , which is composed of the islands of closed contour lines of the potentials. The (Eulerian) statistical characteristics of each geometrical locus were identified.

The time-dependence of the stochastic potential produces anomalous increase of the Lagrangian coherence, instead of the expected decay after the decorrelation time. In particular, the perpendicular average displacements conditioned by ϕ^0 significantly increase and the transitory hidden drifts become long-life structure that survive at $t \gg \tau_c$. The enhanced coherence is found to be associated to a long memory of the Lagrangian potential. Also, the trajectories conditioned by the initial potential become statistically identical for all values of ϕ^0 , not only on the domain of small potential with width Δ , as in frozen potentials. These effects are caused by the stochastic liberation by the time-variation of the potential of the trajectories that initially are trapped, followed by repeated stochastic captures that are constraint by of the approximate invariance of the total potential.

* Electronic address: madalina.vlad@infpr.ro

- [1] Falkovich, G., Gawedzki, K. & Vergassola, M. Particles and fields in fluid turbulence. *Rev. Mod. Phys.* **73**, 913-975 (2001).
- [2] Vassilicos, J. C. Turbulence and intermittency. *Nature* **374**, 408-409 (1995).
- [3] Yamada, T. *et al.* Anatomy of plasma turbulence. *Nature Phys.* **4**, 721-725 (2008).
- [4] Kraichnan, R. H. Diffusion by a random velocity field. *Phys. Fluids* **19**, 22-31 (1970).
- [5] Balescu R., *Aspects of Anomalous Transport in Plasmas*, Institute of Physics Publishing (IoP), Bristol and Philadelphia, 2005.
- [6] Vlad M. & Spineanu F. Trajectory structures and transport. *Phys. Rev. E* **70**, 056304 (2004).
- [7] Vlad, M. & Spineanu, F. Random and quasi-coherent aspects in particle motion and their effects on transport and turbulence evolution. *New J. Phys.* **19** 025014 (2017).
- [8] Kraichnan, R. H. & Montgomery, D. Two-dimensional turbulence. *Rep. Prog. Phys.* **43**, 547-619 (1980).
- [9] Provenzale A. Transport by coherent barotropic vortices. *Annu. Rev. Fluid Mech.* **31**, 55-93 (1999).
- [10] Krommes, J. A. Fundamental statistical descriptions of plasma turbulence in magnetic fields. *Phys. Reports* **360**, 1-352 (2002).
- [11] Weisse, J. & McWilliams J. Temporal scaling behavior of decaying two-dimensional turbulence. *Phys. Fluids A* **5**, 608-621 (1993).
- [12] Spineanu, F. & Vlad, M. Stationary vortical flows in two-dimensional plasma and in planetary atmospheres. *Phys. Rev. Lett.* **94**, 235003 (2005).
- [13] Palade D. I. and Vlad M. Fast generation of Gaussian random fields for direct numerical simulations of stochastic transport, *Statistics and Computing* **31**, 60 (2021).
- [14] Taylor J. B. and McNamara B. *Phys. Fluids* **14**, 1492 (1971).
- [15] Vlad M. and Spineanu F. Hidden drifts in turbulence *Europhysics Letters (EPL)* **124**, 60002 (2018).
- [16] Vlad, M., Spineanu, F., Misguich, J.H. and Balescu, R. Diffusion with intrinsic trapping in two-dimensional incompressible stochastic velocity fields. *Phys.Rev.E* **58**, 7359 (1998).
- [17] Vlad M. and Spineanu F. Combined effects of hidden and polarization drifts on impurity transport in tokamak plasmas *Phys. Plasmas* **25**, 092304 (2018).
- [18] Palade D. I., Vlad M. and Spineanu F. Turbulent transport of the W impurity ions in tokamak plasmas: properties derived from a test particle approach. *Nuclear Fusion* **61**, 116031 (2021).
- [19] Vlad M., Palade D. I. and Spineanu F. Effects of the parallel acceleration on heavy impurity transport in turbulent tokamak plasmas. *Plasma Phys. Control. Fusion* **63**, 035007 (2021).

